DEVELOPMENT AND DESIGN OF CLOSED-CELL ALUMINUM FOAM-BASED LIGHTWEIGHT SANDWICH STRUCTURES FOR BLAST PROTECTION

A Thesis Submitted to
The Graduate School of Engineering and Sciences of
Izmir Institute of Technology
in Partial Fulfillment of the Requirements for the Degree of

MASTER OF SCIENCE

in Mechanical Engineering

by
Çağrı ERGÖNENÇ

July 2008
İZMİR

We approve the thesis of **Çağrı ERGÖNENÇ**

Asst. Prof. Dr. Alper TAŞDEMİRCİ
Supervisor

Prof. Dr. Mustafa GÜDEN
Co-supervisor

Asst. Prof. Dr. Seçil ALTUNDAĞ ARTEM
Committee Member

Asst. Prof. Dr. Cemalettin DÖNMEZ
Committee Member

18 July 2008

Date

Assoc. Prof. Dr. Metin TANOĞLU
Head of the Mechanical Engineering Department

Prof. Dr. Hasan BÖKE
Dean of the Graduate School of Engineering and Sciences

ACKNOWLEDGMENTS

I would like to express my deepest gratitude to my supervisor Asst. Prof. Dr. Alper TAŞDEMİRCİ and my Co-Advisor Prof. Dr. Mustafa GÜDEN for his instructive comments, valued support throughout the all steps of this study and patience to my questions.I am also grateful to the support provided by TÜBİTAK (Project 106M353). I would like express my sincere thanks to Dr. Ian W. Hall, Department of Mechanical Engineering at University of Delaware, for use of the computational facilities. And also I would like to thank my family and Irmak IŞIK for patience and endless support.

TABLE OF CONTENTS

LIST OF FIGURES

Figure **Page**

LIST OF TABLES

Table **Page**

ABSTRACT

DEVELOPMENT AND DESIGN OF CLOSED-CELL ALUMINUM FOAM-BASED LIGHTWEIGHT SANDWICH STRUCTURES FOR BLAST PROTECTION

Blast performance and energy absorption capability of closed-cell aluminum foam based lightweight sandwich structures were investigated by a coupled experimental and numerical technique to find out the effect of face and core material on the blast response. Split Hopkinson Pressure Bar Testing Method (SHPB) was used to characterize the mechanical properties of constituents of the sandwich structures at high strain rates. A SHPB set-up, a high strain rate testing apparatus which can successfully create blast load at laboratory scales, was built at IZTECH on behalf of a TUBITAK project (106M353). The high strain rate test data were used as an input for the numerical models. Closed-cell aluminum foam was chosen as core material for sandwich structures owing to its high energy absorption characteristic while deforming plastically. Finite element modeling of sandwich structures subjected to blast loading were performed for different core and face thicknesses and face materials in order to investigate their effects on the blast load mitigation. Experimentally and numerically revealed conclusions are; sandwich structures absorbed more energies than the bulk materials from %50 to %150 when appropriate combinations of core and face materials are used. Numerical simulations showed that 6.3 and 7.2 cm thick foam interlayer are the most efficient foam thicknesses for a 9 cm sandwich plate against 10 kg TNT blast load. Another important conclusion is for the same blast threat i.e. 10 kg of TNT, AISI 4340 Steel is the most effective face material.

ÖZET

PATLAMAYA KARŞI KAPALI HÜCRELİ ALÜMİNYUM KÖPÜK İÇEREN HAFİF SANDVİÇ YAPILARIN TASARIMI VE GELİŞTİRİLMESİ

Alüminyum köpük içeren hafif sandviç yapıların patlama performansı ve enerji emebilme kabiliyeti, yüzey ve ara malzemelerin sistemin patlamaya karşı verdiği tepkiye etkisi, hem deneysel hem de sayısal teknikler kullanılarak incelenmiştir. Split Hopkinson Basınç Barı (SHBB)Test Metodu sandviç yapının öğelerinin yüksek hızda mekanik özelliklerini karakterize etmek için kullanılmıştır. Bir yüksek hızda deformasyon cihazı olan SHBB, patlama yükünü laboratuar koşullarında başarı ile oluşturabilmektedir. Kullanılan SHBB , İzmir Yüksek Teknoloji Enstitüsü bünyesinde 106M353 kodlu TÜBİTAK projesi kapsamında kurulmuştur. Yüksek hızda deformasyon test verileri ve sonuçları, sayısal modellemede girdi verisi olarak kullanılmıştır. Kapalı hücreli alüminyum köpüğün, plastik deformasyona uğrarken yüksek enerji emme karakteristiğine sahip olması sebebi ile sandviç yapıda ara malzeme olarak seçilmiştir. Sandviç yapının öğeleri olan yüzey ve ara malzemelerin kalınlıkları ve yüzey malzemesinin patlama ilerlemesine etkisi sonlu eleman modellemeleri yapılarak incelenmiş ve karşılaştırılmıştır. Deneysel ve sayısal deneyler sonucunda açığa çıkan sonuçlar; sandviç yapılar uygun ara ve yüzey malzeme kombinasyonu oluşturulduğu zaman, aynı ağırlıktaki yekpare malzemeden yaklaşık %50-%150 daha fazla enerji emebilmektedir. Sayısal çözümler göstermektedir ki, 9 cm'lik bir sandviç yapıda, 10 kg TNT lik patlama yükü karşısında, 6.3 cm ve 7.2 cm lik alüminyum köpük ara yüzey malzemesi en verimli köpük kalınlığıdır. Diğer önemli bir sonuç ise, aynı patlama yüküne karşı en verimli yüzey malzemesi AISI 4340 çeliğidir.

CHAPTER 1

INTRODUCTION

The last years have witnessed an increase number of wars, internal disorders, terrorism and conflicts between civilians and military forces. Bosnia and Iraq are two recent vivid examples. The weapons used in these wars are highly technical, easy to manufacture with today's technologies and relatively cheap. Moreover, the abilities of weapons to kill the living creatures are constantly increasing day by day. One of the examples of the cheap, easy to produce and portable weapons is landmine. 80 million landmines are estimated to be buried worldwide (LandMineSurvivorsNetwork). 54 countries have approximately 180 million antipersonnel mines stockpiled and more than 200,000 square kilometers of the world's surface is contaminated with landmines. The landmines kill or injure 15,000–20,000 persons annually, including civilians and soldiers (Organization 2004) (Stamatios et al. 2006).

In recent years, blast protection and energy absorption structures have been taken considerable interest from both military and civil industries. The protection of humans as well as the structures particularly military structures such as lightweight-armored-vehicles in the event of a detonation of landmine is an important and challenging issue.

The blast protection structures are commonly manufactured in the form of sandwiches which have been known for several decades with their excellent energy-absorbing capabilities. A sandwich structure consists of a light-weight core material and two sheets materials, one at the front and one at the back face of the core. The core materials are usually made from foams due to their low weight, being less than that of same bulk material. Owing to this, it is possible to design foam cored sandwich structures showing the much more energy absorbing property than bulk material, but with significant weight savings.

Closed-cell aluminum foam offers a combination of properties including low density, high specific stiffness and strength, and high energy absorption. The deformation of foam proceeds with localized deformation leading to almost a constant plateau stress. The aluminum-foam core sandwich structure was previously tested in

integral lightweight armor and found to reduce the dynamic deflection of the backing plate than the base line. Owing to their abilities to deform large strains and relatively high energy absorbing capabilities aluminum closed-cell foams have quite high potentials to be used as core material in lightweight blast resisting structures particularly in defense industry.

1.1. Fundamentals of blast protection

1.1.1. Blast Phenomena

After detonation of explosives, a shock wave expands outward in the surrounding air from the detonation point. This shock wave is called "blast wave". The distance between center of explosion and the blast face of the structure is called standoff distance as shown in Figure 1.1. The blast wave magnitude depends on Standoff distance. Figure 1.2 shows a typical pressure-time history of a blast wave. The peak overpressure is reached instantly upon arrival of the blast wave, and then the magnitude starts to decrease gradually until a negative pressure phase. This negative pressure phase is called as suction phase and commonly is omitted in the design and analysis.

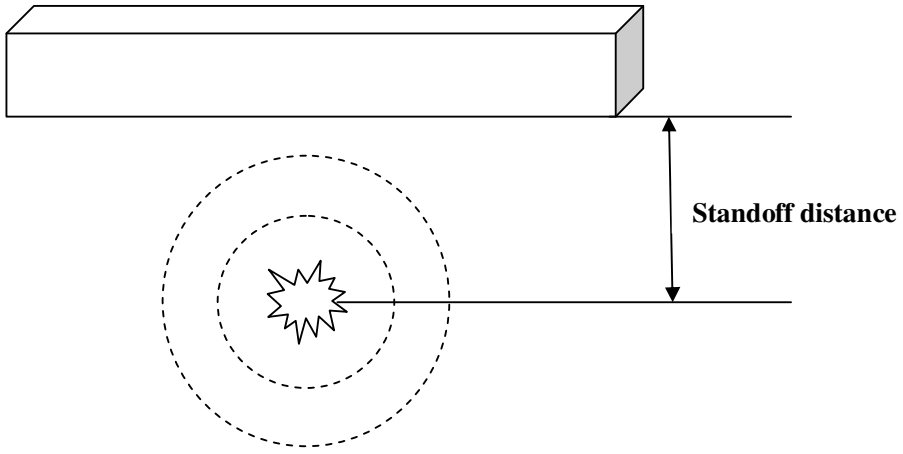

Figure 1.1. Schematic view of Standoff distance

The impulse, which is occurred by the detonation, is calculated as the area under the pressure-time curve from arrival time (t_a) to the end of positive phase (t_b),

$$I = \int_{ta}^{tb} p(t)dt \qquad (1.1)$$

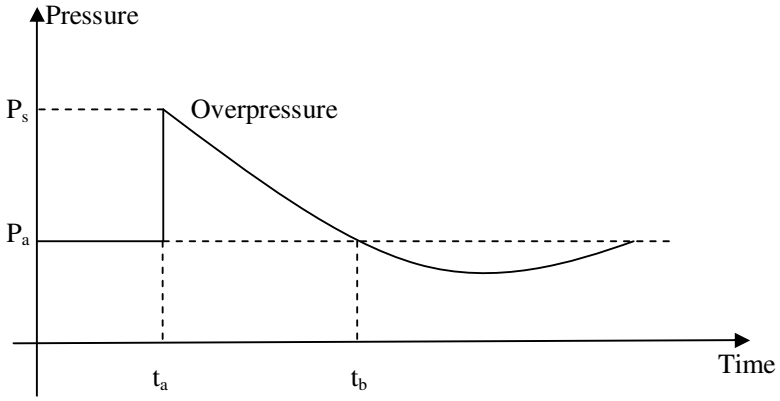

Figure 1.2. Blast wave pressure-time history

1.1.2. Sandwich structures and closed-cell aluminum foam

A typical sandwich structure (Figure 1.3) consists of two surface plates connected by a lightweight core material. The components of the sandwich material are bonded together using either adhesives or mechanical fasteners. In a typical sandwich structure, there are two faces which are generally made from the same material and in the same thickness. The face sheets primarily resist the in-plane and lateral loads. However, in special cases the faces may differ in thickness, material or any combination. The core of a sandwich structure can be any material or in architecture. In general, there are four type cores: foam or solid core, honeycomb core, truss core and web core.

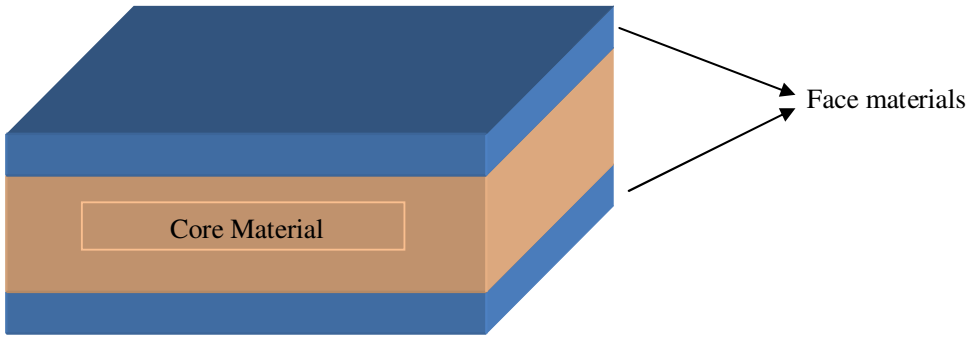

Figure 1.3. A typical sandwich structure

The use of sandwich structures is increasing steadily. The applications include blast protection structures, satellites, automobiles, aircraft, ships, rail cars, wind energy systems and constructions (Vinson 2005). The need for high performance and low-weight structures ensure that sandwich structures applications would continue. The advantages of sandwich construction include

- high load bearing capacity at low weight
- high energy absorbing capability
- excellent thermal insulation
- crack growth and fracture toughness characteristics are better compared to solid laminates
- surface finished faceplates provide good resistance against aggressive environments
- long life at low maintenance cost
- good water and vapor barrier
- excellent acoustic damping properties

Closed-cell metal foams have been developed since about 1990. The size of the pores or cell size is usually between 1 and 8 mm. One of the widely used closed-cell metal foams is made from aluminum. Al closed-cell foams are materials of increasing importance because they have good energy absorption capabilities combined with good thermal and acoustic properties. Al foams can absorb a much larger quantity of

mechanical energy than the bulk Al. Al foams are fire resistant and can be easily recycled and float on water because density of closed-cell aluminum foams is less than 1g/cc. Closed-cell Al foams are widely used in civilian, military and industrial applications. Lightweight armor, mine blast containment, water-tight doors on ships, firewalls, energy absorbing bumpers, door side impact bars, front crash rails space frame components are some examples for the aluminum foam applications.

1.2. Background

The blast performance of sandwich structures is becoming more popular day by day, many authors have been publishing significant amount of papers in this field. In his study, Mukherjee et al. (1999) carried out a number of blast experiments on sacrificial layered claddings to investigate the performance of sandwich structure under blast loading. He also studied the same problem analytically and numerically and compared the results with those of the real tests. He reported that the layers collapsed successively in the same manner as predicted in the analytical studies. The collapse mode of the unit cell was always the same as predicted in the analytical studies. However, collapse of the layers was slower than predicted in the analytical studies. They also showed that experiments the efficacy of the layered sacrificial claddings in design of blast resistant structures.

Boyd et al. (2000) carried out blast experiments on a fixed steel plate subjected to blast loading. He investigated the acceleration, pressure loading and displacement histories both experimentally and numerically.

Hanssen et al. (2001) conducted the full-scale ballistic pendulum tests of aluminum foam panels and investigated the blast performance of those panels. He observed that the energy and impulse transfer increased by adding foam panel to the pendulum.

Hutchinson et al. (2003) proved that sandwich structures had higher shock resistance than bulk material plates in equal mass criteria. His study was completely analytical and he used a dynamic finite element formulation to analyze the plate response.

Lee et al. (2004) numerically investigated the response of the honeycomb core sandwich structures subjected to blast loading and optimized the structure in terms of energy absorption.

Micheal et al. (2004) analyzed the imparted impulse from a blast loading for energy absorbing materials numerically. He compared the Lagrangian-Eulerian and the Conwep air blast functions and showed that Conwep air blast function showed similar deformation patterns compared to real experiments.

Vaidya et al. (2004) investigated the behavior of aluminum foam sandwich plates exposed to blast loading. They reported that the composite failed under bending and the failure was dominated by shear strain. They found that the reason of failure of sandwich structure was core failure and matrix failure in the laminate.

Veldman (2004) analyzed the effects of static pre-pressurization on the blast-induced deformation of aluminum plates by using both numerical and experimental methods. He concluded that the pre-pressurization had not a significance effect on the blast damage of the plates.

Yen et al. (2005) numerically studied the effect of honeycomb core strength on energy absorption during blast loading. He concluded that sandwiches having higher core strength values absorbed more energy.

The blast response of sandwich structures was studied by Radford et al. (2005). He reported that sandwich structures showed higher shock resistance than bulk material plates in equal mass criteria. He also showed that the shock resistance increased while core thickness increasing. Hutchinson et al. (2003) also found out a similar conclusion analytically.

Fleck et al. (2006) developed an analytical model to classify the impulsive response of sandwich beams based on the relative time-scales of core compression and the bending/stretching response of the sandwich beam. They showed that an overlap in time scales led to a coupled response and possibility of an enhanced shock resistance. They compared the predictions of the analytical model with finite element simulations of impulsively loaded sandwich beams comprising an anisotropic foam core and elastic, ideally plastic face-sheets. They found that the analytical and numerical predictions were in good agreement up to the end of core compression and the optimal core strength depends on the level of blast impulse, with higher strength cores required for greater blasts.

1.3. Objective and method

The objective of this thesis is to investigate the blast performance and energy absorption capability of the sandwich structures subjected to blast loads, and to find out the effect of face and core material on the blast response. A coupled numerical and experimental study was conducted. High strain rate mechanical properties of the materials comprising the sandwich structure were obtained from the Split Hopkinson Pressure Bar set-up. SHPB set-up, a high strain rate testing device which can mimic the blast load at laboratory scales, was established at IZTECH in a TUBITAK project coded as 106M353. The high strain rate test data were used as an input for the numerical models. Detailed numerical simulations series were performed on the blast loading of a series of sandwich structures varying in foam density, foam core and face material thicknesses and face material types (Titanium, aluminum, and steel, composite) in order to investigate their effects on the blast load mitigation.

CHAPTER 2

EXPERIMENTAL INVESTIGATION

This chapter focuses on material manufacturing, sample preparation and Split Hopkinson Pressure Bar (SHPB) testing. A brief theoretical background of the SHPB theory is also given, for example calculation of the specimen stress, strain, and strain rate. The basics of various testing precautions and data acquisition procedures are described briefly as well.

2.1. Materials and sample preparation

2.1.1. Fabrication of polyester matrix composite

E-glass/Polyester composite plates were produced using infusion (VARTM-vacuum assisted resin transfer molding) process. Infusion process is widely used in composite production because of its superior properties such as; high part quality and reproducibility, reduced production costs, the lower need of investments in tooling and machinery and etc.

In the composite preparation, the number of laminates to obtain an intended thickness was calculated using the following equation,

$$n = \frac{T \times \rho f \times Vf}{mof} \tag{2.1}$$

where, T is thickness of final plate, mof is surface mass of the fiber, ρ_f is density of the fiber, Vf is fiber volume fraction and n is the number of the laminates to achieve the thickness of the final plate.

The mass of resin to form the composite was calculated as,

$$m = \rho m \times Vm * V \tag{2.2}$$

where, ρm is density of the resin, Vm is volume of the matrix, and V is the theoretical volume of the plate.

The infusion process was carried out in the following sequence. The process was performed on a glass plate. The glass plate was cleaned and waxed before infusion the resin. The wax was to create a regular and smooth surface. Fibers were cut in calculated dimensions and weighted. The infusion set-up is shown in Figure 2.1. The set-up consists of lay-up fibers, draining tissue, delaminate tissues, resin and vacuum ramp, vacuum bag and vacuum pipes. The parts were sequentially inserted on the fiber lay-up. The vacuum bag was taped from all sides for proper vacuuming. The polyester resins mixed with hardener and the infused to the infusion set-up.

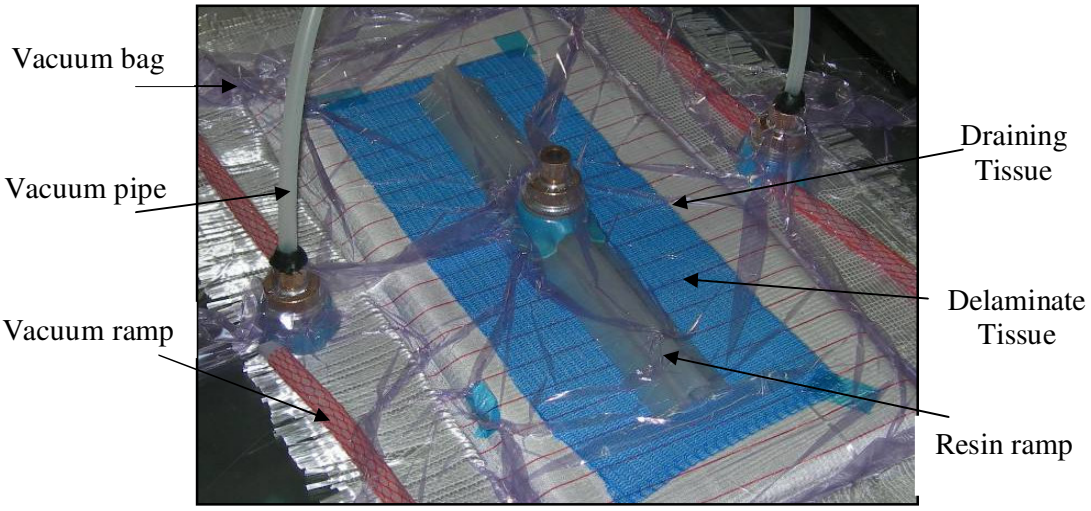

Figure 2.1. Infusion scheme

In this investigation, three different fiber lay-ups, “0/90 E-glass bi axial”,”45/-45 E-glass bi axial “,”0/45/90/-45 E-glass” were used. As a polyester resin, CRYSTIC 703 PA was used to perform process because of its having a compatibility of vacuuming.

2.1.2. Fabrication of closed-cell aluminum foams

Aluminum closed cell foams were prepared using the foaming powder compacts (precursors) process. This process is patented by Fraunhofer CMAM (Baumeister . 1996, Baumeister. 1997, Baumeister. 1991). The main step in the foaming process is shown in Figure 2.2. The process starts with mixing Al and TiH_2 (1 wt%) powder. The average particle size of the Al powder used were 34.64 and 22.36 □m, respectively and the size of TiH_2 particles was less than 37 □m. The specification of raw materials is listed in Table 2.1. The powder mixture was cold compacted inside a steel die, 70x70 cm in cross-section under a pressure of 200 MPa. The compacts of 80% relative density were hot-forged at a temperature of 350 ^{o}C. After hot-forging the resulting foamable precursor material relative density reached 98%. The thicknesses of the foamable precursor plates were approximately 8 mm (Figure 2.3(a)). Before foaming, the cross-sectional area of hot-forged precursor was machined into the dimensions of 70x70 mm. same with the cross-sectional dimensions of the foaming molds. Foaming was done in a in a furnace at a temperature of 750 ^{o}C inside a steel die which had the same cross-sectional area with that of the precursor. The die was pre-heated and then the precursor was inserted into the die. The expansion of the precursor started after 5 min and filled the die completely at about 7 min.

Cylindrical compression test specimens, 20 mm in diameter and 20 mm in length, were core-drilled form the foam plates using electro-discharge machine normal to the foaming direction (Figure 2.3(b)). The samples were weighed before compression testing in order to calculate relative densities. The relative density, ρ^*, is calculated using following equation,

$$\rho^* = \frac{\rho_f}{\rho_s} \tag{2.3}$$

where, ρ_f and ρ_s refer to the foam and bulk alloy densities, respectively. Compression tests on the foam samples were conducted using a Schitmatzsu AGX testing machine at a cross-head speed of 0.1 mm s^{-1}.

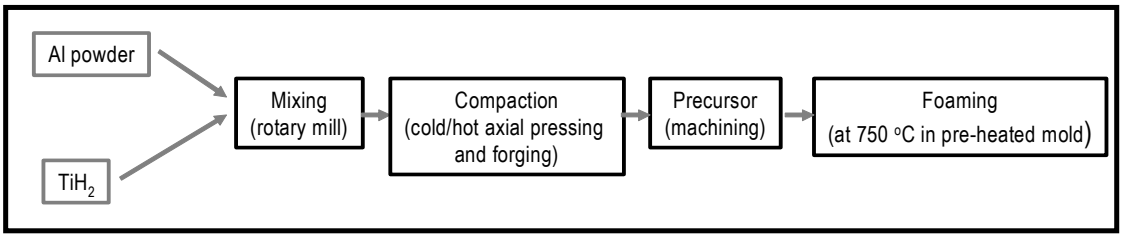

Figure 2.2. The schematic of foaming powder compact process

Table 2. 1. Specifications of raw materials of aluminum foam

Material	**Size**	**Purity**
Al powder (Aldrich)	< 74 μm	99%
TiH_2 (Merck)	< 37 μm	>98%

.

(a) (b)

Figure 2.3. Pictures of (a) cold compacted foamable precursor and (b) core-drilled foam plate

2.1.3. Test Sample Preparation

Composite plates prepared were surface grinded to their final thicknesses. Cubic test samples were then cut from the composite plates. The samples were tested through x, y and z directions (Figure 2.4). Foam samples were prepared using electro-discharge machine in order to not to damage the cells. The cylindrical samples were cut normal to the foaming directions of the foamed plates.

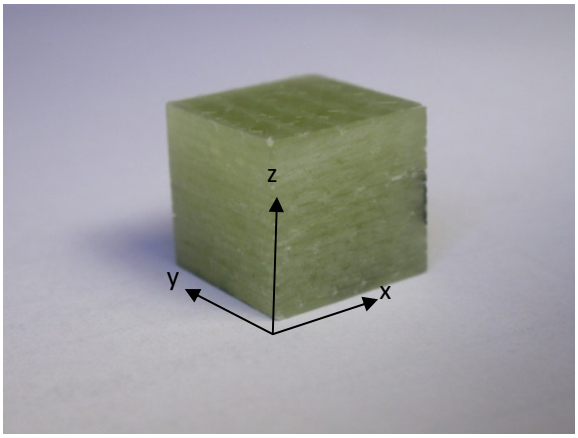

Figure 2.4. Test directions of composite samples

2.2 . High strain rate testing

2.2.1. Split Hopkinson Pressure Bar (SHPB) theory and experiments

SHPB is a widely used testing method for the characterization of the dynamic mechanical properties of metals, composites, foam-like materials, plastics and other materials. SHPB apparatus consists of striker, incident and transmitter bar and the specimen to be tested. The system is shown schematically in Figure 2.4. A gas gun accelerates the striker bar that hits the incident bar. A specimen is sandwiched between the incident and transmitter bar and a rectangular compression wave with well-defined amplitude and length is generated in the incident bar, called incident wave. When this wave reaches the specimen part of it is transmitted into the specimen and into the transmitter bar which is called transmitter wave, and the rest is reflected back to the incident bar. Incident and transmitter bars are instrumented with strain gages at the same distances from the specimen. Using a one-dimensional wave propagation analysis (Tasdemirci 2007), it is possible to determine high strain rate stress-strain curves from measurements of strain in the incident and transmitter bars.

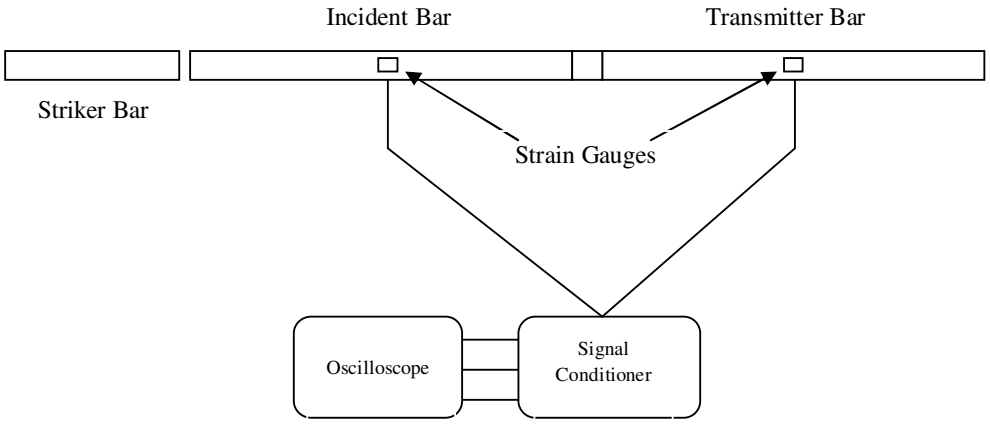

Figure 2.5. Schematic view of SHPB

2.2.2. Specimen stress, strain and strain rate calculation

SHPB principles are based on uniaxial elastic wave propagation in long bars. When a long bar having a velocity of v_o strikes another a stationary long bar (Figure 2.5) having the same elastic modulus and diameter as the impact bar, a rectangular elastic stress pulse is produced as shown in Figure 2.6.

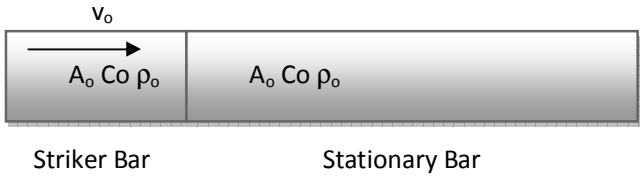

Figure 2.6. Collision of two identical bars

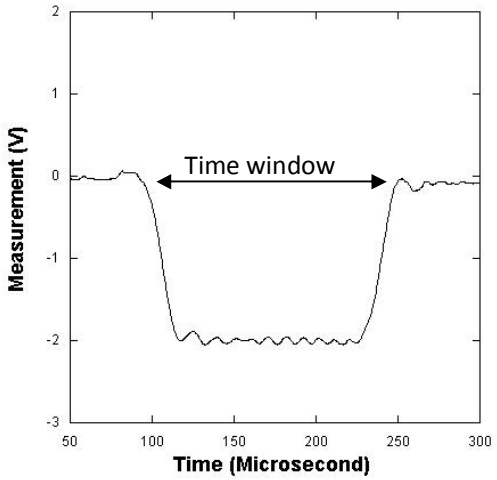

Figure 2.7. Produced rectangular pulse

In the incident bar, the magnitude of stress and strain are direct functions of the velocity of the striking bar, modulus (E) and elastic wave velocity (C) of the impacted bar. The maximum stress (σ) and the maximum strain (ε) in the bar are given as follows;

$$\sigma_b = C_b \rho_b u \tag{2.4}$$

$$u = \frac{v_o}{2} \tag{2.5}$$

$$\sigma_b = C_b \frac{E_b}{C_b^{\,2}} \frac{v_o}{2} = \frac{E_b v_o}{2C_b} \tag{2.6}$$

$$\varepsilon_b = \frac{\sigma_b}{E_b} = \frac{v_o}{2C_b} \tag{2.7}$$

The total time period in which the incident pulse operates is called the time window (T_w) and given as;

$$T_w = \frac{2L_{SB}}{C_b} \tag{2.8}$$

where; L_{SB} is the striker bar length.

Kolsky (1949) developed the following relation for calculating the specimen stress.

$$\sigma_s(t) = E\frac{A_0}{A}\varepsilon_T(t) \tag{2.9}$$

where; E is the transmitter bar's elastic modulus, A_o is the output bars cross sectional area, A is the sample's cross sectional area, and $\varepsilon_T(t)$ is the transmitted strain history. Specimen strain rate is calculated as;

$$\frac{d\varepsilon_s(t)}{dt} = -\frac{2C_0}{L}\varepsilon_R(t) \tag{2.10}$$

where; $\varepsilon_R(t)$ is the reflected input bar strain history, L is the specimen length prior to impact, and C_0 is the infinite wavelength wave velocity in the incident bar, calculated from elementary vibrations as;

$$Co = \sqrt{\frac{E}{\rho}} \tag{2.11}$$

where; E and ρ are the bars elastic modulus and density. It is assumed that the wave propagation effect in the small sample may be neglected so strain of the specimen equation is written as;

$$\varepsilon(t) = -\frac{2C_0}{L}\int_0^t \varepsilon_R dt \tag{2.12}$$

2.2.3. Building SHPB at IYTE

During the design process, numerical modeling was used as a strong tool to adequately select the dimension of the striker, incident and transmitter bars. SHPB was modeled for various lengths and diameters of aforementioned components of the system. According to these results, optimum bar lengths which provide one wave stress

propagation and minimum stress wave dispersion were established. Also mentioned that, transmitter bar length is taken as half of the bar length to guarantee to get loading for once in sample.

The effect of striker bar length on stress wave created in incident bar is shown in Figure 2.7. As the striker bar length increases, time window of the wave increases. These numerical analyses showed that 350 and 700 mm long striker bar can produce required stress wave profile. Components were manufactured in the dimensions accordingly to the numerical simulations. Bar response of the designed SHPB set-up for 3 different striker speeds when a ceramic sample is tested, is given in Figure 2.8.

CPM Rex 76 was selected as bar material because of its high dynamic mechanical properties (Table 2.2). According to the SHPB theory in order to keep the tests as valid, bar material needs to be remained elastic during all the tests done.

Table 2.2. Mechanical Properties of CPM Rex 76

Material	Elastic Modulus	Yield Strength	Density	Hardness
CPM Rex76	214 GPa	700 MPa	8255 kg/m^3	40 HRC

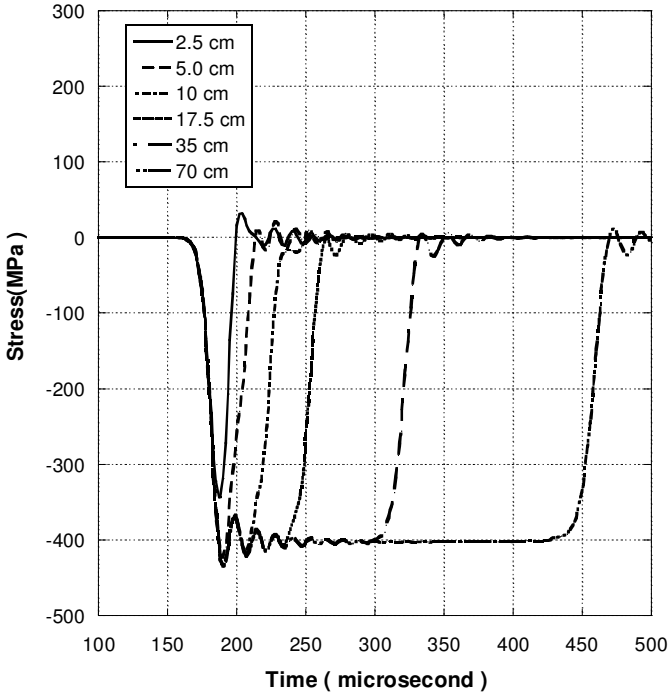

Figure 2.8. Stress behavior of incident bar corresponding to striker bar length

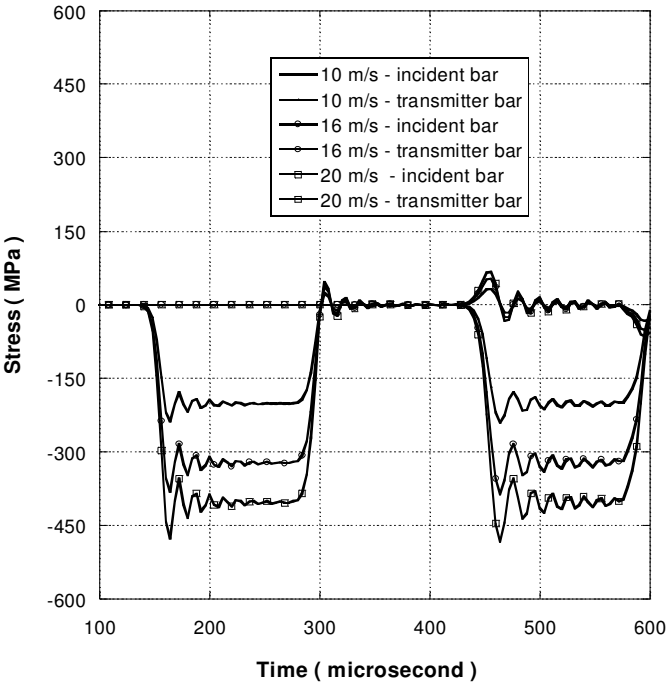

Figure 2.9. Stress behavior of incident bar corresponding to striker bar velocity

SHPB Testing Apparatus consists of 4 main parts (Figure 2.9); girder, bar supporters, stopper and gas gun. Bar support apparatus, gas gun and stopper sit on the girder. Girder is wheeled to transport the system easily from one place to another. Bars and gas gun are centered by bar supporter. The stopper absorbs the excessive energy of the bar.

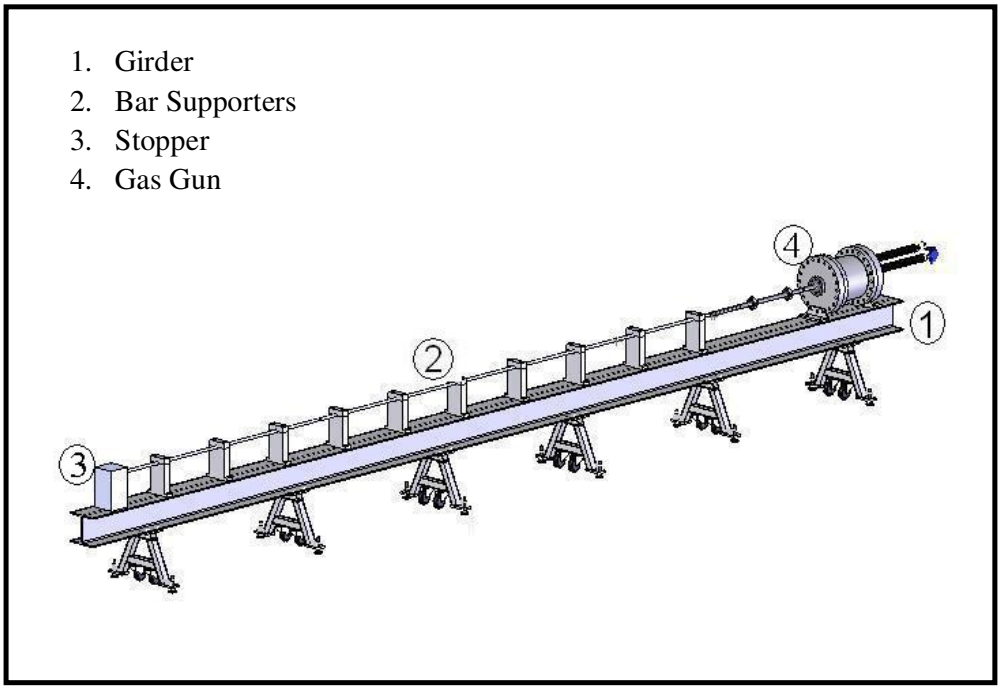

Figure 2.10. Schematic view of SHPB

After a long design period, the construction of SHPB and gas gun was started. Gas gun was designed and manufactured to resist 15 bars of pressure and it was tested under hydrostatic pressure. During the test, gas gun was filled with water and 25 bars of pressure was applied by an external test pump, system was kept at that pressure for 30 minutes and the joints was checked for leak.

During the construction, initially the girder was cut to the required length. Then, bar supporters were CNC machined from aluminum. Teflon was used for centering the axis of the bars with that of the gas gun because of its having low friction coefficient and high machinability. The stopper was machined from steel. Finally all these parts and gas gun were assembled

After all these processes SHPB and gas gun were assembled (Figure 2.10).

Figure 2.11. Photo of SHPB

2.2.4. Test procedure

In order to do a valid test, one dimensional stress wave must propagate in the incident and transmitter bars. One of the most important experimental factors assuring one-dimensional wave propagation is bar alignment. If the striker bar impacts to the incident bar face non-centered or at an angle, non-uniform wave propagation occurs. This is also valid for the incident bar-sample and transmitter bar-sample interfaces. There has to be a thin grease film between the bar ends and specimen in order to reduce frictional forces.

A typical testing procedure is as follows;

1. Align the bars
2. Measure the specimen dimensions
3. Apply lubricant on sample and bar ends

4. Sandwich the specimen between the bars
5. Adjust the pressure of gas chamber
6. Set the oscilloscope and strain gauge conditioner parameters
7. Fire the gas gun
8. Transfer data from oscilloscope to PC
9. Reduce the data
10. Plot the stress vs. strain curve

2.3. Static Testing

Static testing was also performed so as to compare results with those of the high strain rate tests and use them as input in FE modeling. These tests were conducted on a universal mechanical testing machine SHIMADZU AG-X (Figure 2.11) in Dynamic Testing and Modeling Laboratory of IZTECH.

Figure 2.12. SHIMADZU Mechanical testing machine

CHAPTER 3

FINITE ELEMENT MODELING

3.1. Model Description

In this study, 50x100 cm flat rectangular sandwich panels were subjected to blast loading with a constant standoff distance. The commercial explicit finite element code LS-DYNA971 was used for investigating the three dimensional dynamic response of the sandwich structure to blast loading. A standoff distance of 30 cm was used (the distance between a land mine and down side of a light weight armored vehicle) as shown in Figure 3.1. The panel was clamped at all four edges and was modeled as quarter model with using appropriate boundary conditions to reduce solution time. Three components were created as back face, core and front face. The back face plate is referred as blast face so wave front of the blast pressure directly strikes to this face.

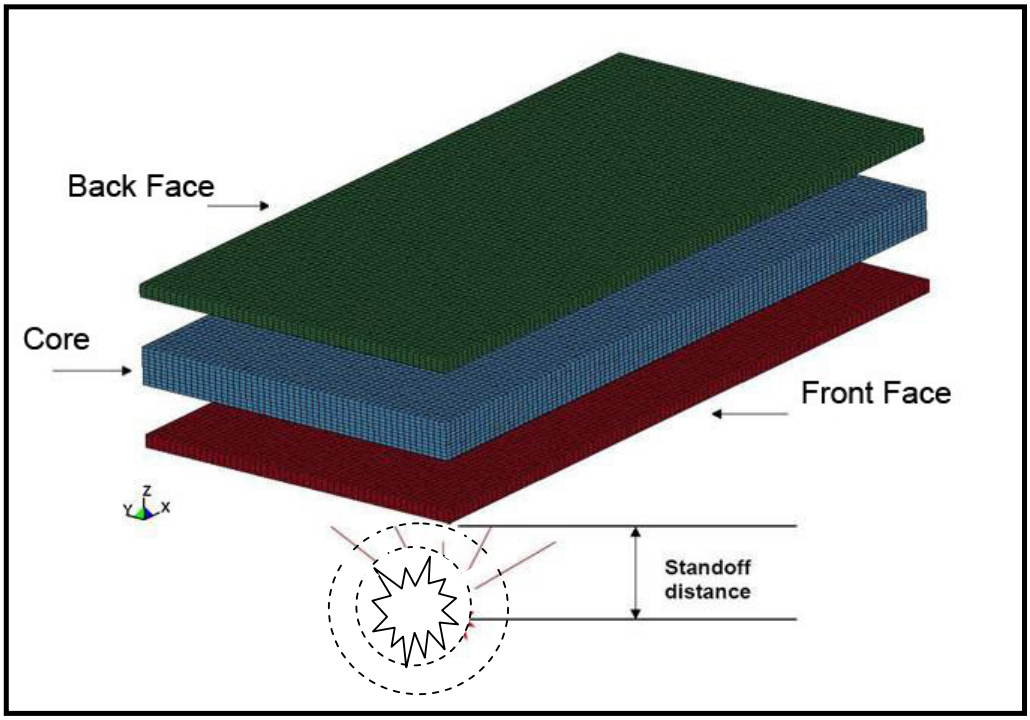

Figure 3.1. Schematic view of modeled sandwich structure

This model was meshed with brick solid elements and the total number of elements varies between 90000 and 200000. The material model 3 (MAT_PLASTIC_KINEMATIC) was used for all metal layers (Aluminum 5083-H112, AISI 4340 Steel). Plastic Kinematic material model is one of the commonly used material models in impact and blast simulations. This model is a strain rate dependent elastic–plastic model. In this model, strain rate is accounted for using the Cowper–Symonds model which scales the yield stress by the strain rate dependent factor (14).

$$1 + (\frac{\dot{\varepsilon}}{C})^{\frac{1}{p}} \tag{3.1}$$

where $\dot{\varepsilon}$ is the strain rate. And elastic-plastic behavior of the model is given in Figure 14.

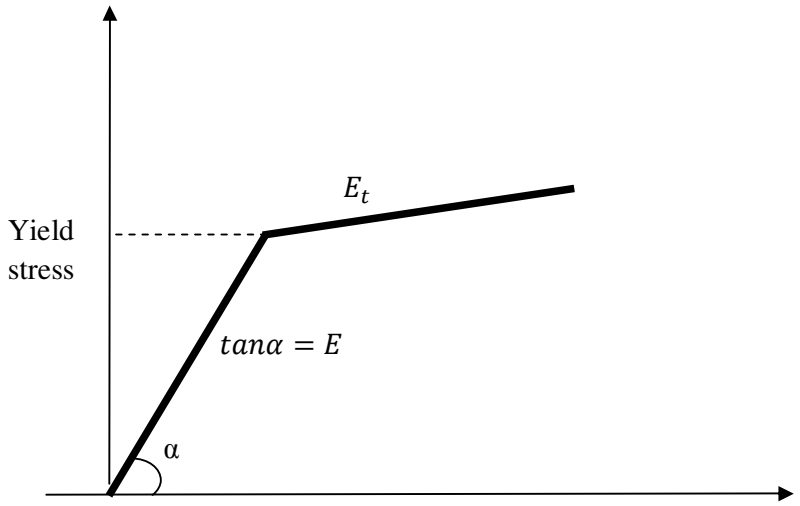

Figure 3.2. Elastic-plastic behavior of MAT_PLASTIC_KINEMATIC

where E_t is the slope of the bilinear stress-strain curve

Material model 15 (MAT_JOHNSON_COOK) was used to model Ti6Al4V (Titanium) face. This material model is strain and temperature sensitive plasticity and used for problems where strain rates vary over a large range. Typical applications include explosive metal forming, ballistic penetration and impact.

Johnson-Cook material model expresses the flow stress as

$$\sigma_y = \left(A + B\bar{\varepsilon}^{p^n}\right)(1 + cln\varepsilon^*)\left(1 - T^{*^m}\right) \tag{3.2}$$

where; A, B, C, n and m are input constants, $\bar{\varepsilon}^p$ is effective plastic strain,

$$\varepsilon^* = \frac{\bar{\varepsilon}^p}{\varepsilon_0} \tag{3.3}$$

is effective plastic strain rate for ε_0=1 s^{-1}.

T^*= (T - T_{room}) / (T_{melt} - T_{room}) is homologous temperature.

The strain at the fracture is expressed as;

$$\varepsilon^f = \left[D_1 + D_{2exp}D_3\sigma^*\right][1 + D_4 ln\dot{\varepsilon}^*][1 + D_5 T^*] \tag{3.4}$$

where σ^* is the ratio of pressure divided by effective stress. Fracture occurs when the damage parameter D reaches the value of 1.

Aluminum foam was modeled with material model 26 (MAT_HONEYCOMB). This material model is commonly used for honeycomb and foam materials with real anisotropic behavior. Material Model 26 uses a local coordinate system that is defined by user. One of the axes of the local system coincides with the extrusion direction of the honeycomb in the undeformed configuration. In this model, elastic modules of local a, b, c-directions vary, from their initial values to the fully compacted values at Vf, linearly with the relative volume V(ratio of the current volume to initial volume).

$$\left.\begin{aligned} \mathrm{E_{aa}} &= \mathrm{E_{aau}} + \beta(\mathrm{E} - \mathrm{E_{aau}}) \\ \mathrm{E_{bb}} &= \mathrm{E_{bbu}} + \beta(\mathrm{E} - \mathrm{E_{bbu}}) \\ \mathrm{E_{cc}} &= \mathrm{E_{ccu}} + \beta(\mathrm{E} - \mathrm{E_{ccu}}) \\ \mathrm{G_{ab}} &= \mathrm{G_{abu}} + \beta(\mathrm{G} - \mathrm{G_{abu}}) \\ \mathrm{G_{bc}} &= \mathrm{G_{bcu}} + \beta(\mathrm{G} - \mathrm{G_{bcu}}) \\ \mathrm{G_{ca}} &= \mathrm{G_{cau}} + \beta(\mathrm{G} - \mathrm{G_{cau}}) \end{aligned}\right\} \tag{3.5}$$

where

$$\beta = \max\left[\min\left(\frac{1 - \mathrm{V}}{1 - \mathrm{V_f}}, 1\right), 0\right] \tag{3.6}$$

And G is the elastic shear modules for the fully compacted honeycomb material

$$\mathrm{G} = \frac{\mathrm{E}}{2(1 + \mathrm{v})} \tag{3.7}$$

In this model, user must define curves that define the magnitude of the average stress versus volumetric strain. A typical stress versus strain curve for model is Figure 3.3.

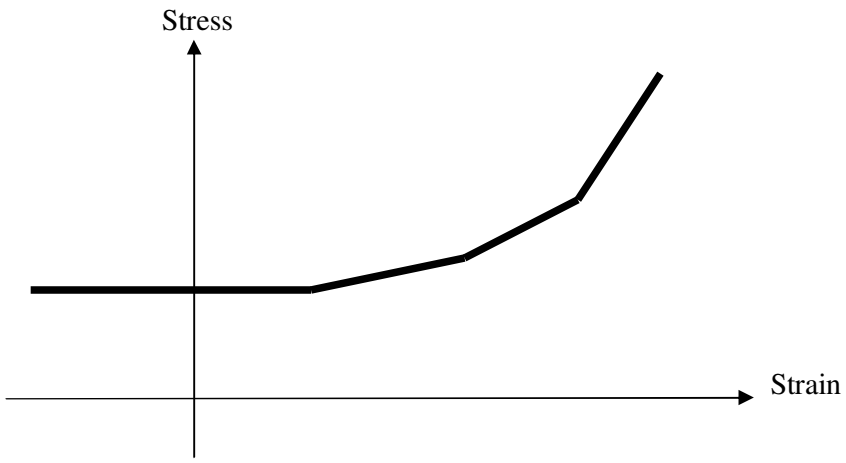

Figure 3.3. A typical stress versus strain curve for MAT_HONEYCOMB

In this study, another investigated topic was composites' impact behavior under blast loading. To achieve purposed result, 20-layer-composite plate was modeled. Dimensions of the plate were 20x20 cm with 2 cm thickness. It was modeled as plate instead of sandwich structure. Because used material model for composite (Mat 162 MSC_DAMAGE) is a very complex material model and it needs too much computational power. The plate was supported by a rigid ring as rigid support from back plate as seen Figure 3.4. A standoff distance of 30 cm was used. To achieve most convenient glass fiber lay-up for blast loading, three type of orientated glass fiber was used. These were "0/90","45/-45" and "0/90/45/-45".

The laminated composite layer was modeled using material model 162 (MSC_DAMAGE) with constant stress solid element formulation. This material model is used to model the progressive failure analysis for composite materials consisting of unidirectional and woven fabric layers.

The material constants used are given in Table 3.1 and the details of the mechanical properties are given in Chapter 4 of this thesis.

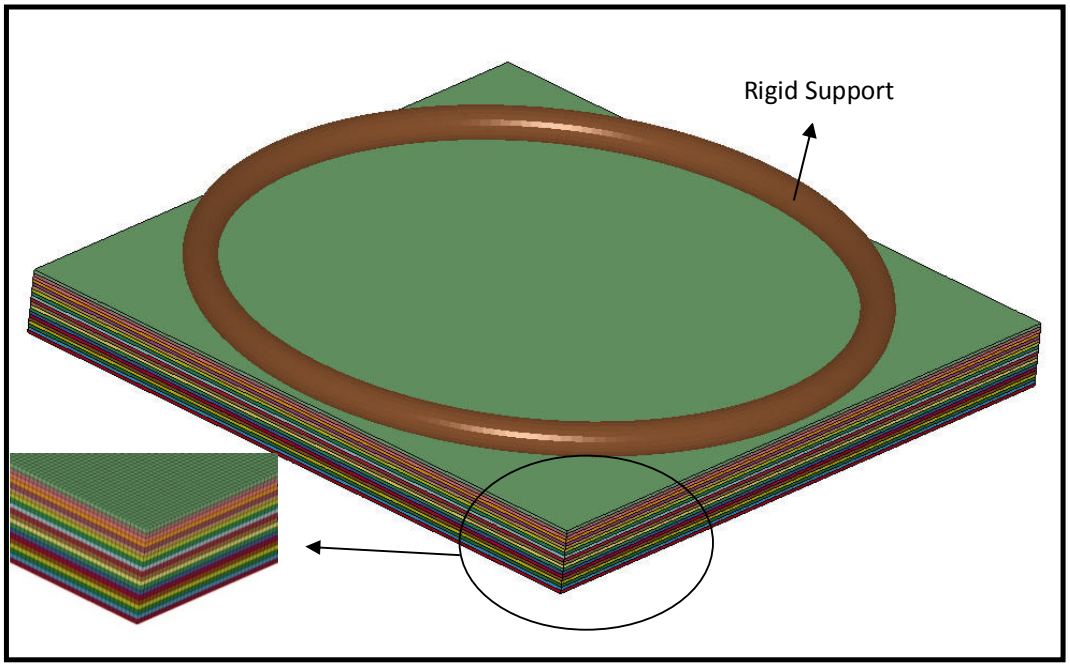

Figure 3.4. Modeled laminated composite

Table 3.1. Material constants used in material model

Material model 3 (MAT_PLASTIC_KINEMATIC)					
Face Material	**Elastic Modulus**	**Mass Density**	**Poisson's Ratio**	**Yield Stress**	**Tangent Modulus**
Aluminum 5083	70.3 GPa	2660 kg/m3	0.33	190 MPa	567 MPa
Steel AISI 4340	196 GPa	7.85 kg/m3	0.3	1550 MPa	2721 MPa

(cont. on next page)

Table 3.1. (cont.) Material constants used in material model

Material model 15 (MAT_JOHNSON_COOK) for Ti6Al4V					
Elastic Modulus	**Shear Modulus**	**Mass Density**	**Poisson's Ratio**	**A**	**B**
114 GPa	44 GPa	4300 kg/m3	0.33	896 MPa	656 MPa
n	**C**	**m**	**Melt Temperature Tm**	**Room Temperature**	**Specific Heat**
0.5	1280 MPa	0.8	1600 ºC	20 ºC	0.5263 J/g-°C

Material model 26 (MAT_HONEYCOMB) for Aluminum foam					
Elastic Modulus	**Mass Density**	**Poisson's Ratio**	**Yield Stress**	**Relative Volume (Vf)**	**Material Viscosity Coefficient**
69 GPa	438 kg/m3	0.285	104 MPa	0.29	0.05
E_{aau}	E_{bbu}	E_{ccu}	G_{abu}	G_{bcu}	G_{cau}
177 MPa	177 MPa	177 MPa	69 MPa	69 MPa	69 MPa

*CONTACT_AUTOMATIC_SURFACE_TO_SURFACE_TIEBREAK and *CONTACT_ERODING_SINGLE_SURFACE_ID were used to define contacts between all components.

Since there is no intention of investigating the effect of soil and some other soil related parameters, blast loading can be assumed as an air blast load. For this purpose ConWep function can successfully represent the blast load investigated. It is a blast pressure function and blast load can be calculated using this function. ConWep function was developed by the US Army in 1991. In this function, pressure is calculated based on the following equation (F. Zhu 2007);

$$P(\tau) = P_r.\cos^2\theta + P_i.(1 + \cos^2\theta - 2\cos\theta) \quad (3.8)$$

where θ is angle of incidence, P_r is reflected pressure and P_i is incident pressure. In this thesis, ConWep air blast function was used to apply blast loading. For this purpose, *LOAD_BLAST card was defined. The used units in model are gram (g), centimeter

(cm), microsecond (μs). Due to using these units on *LOAD_BLAST card IUNIT was set to 4. According to Cole (Cole 1948), the amount of explosive charge in terms of weight is converted to an equivalent value of TNT weight. Due to fact that in this card, the mass of the explosive is defined as equivalent mass of TNT. In this study, for sandwich panel, two-land-mine equivalent explosive was chosen. Equivalent mass of a land mine is about 5000 g TNT so in the LOAD_BLAST card a 10000 g mass of TNT used for the explosive. 10 kg of TNT produces a pressure pulse of 254.378 MPa and also it can be observed from the numerical simulation that the peak pressure occurred at time 51.56 microseconds. For laminated composite panel, blast load was chosen 500 g TNT. 500g of TNT produces a pressure pulse of 54.1 MPa and also it can be observed from the numerical simulation that the peak pressure occurred at time 78.16 microseconds.

For all of the models and solutions, termination time was chosen 2000 microseconds. Time-step of the model was set as default settings.

The energy data can be printed in LS-DYNA file forming a useful check in analysis. The following equation is the energy conservation criteria at all times;

$$E_{kin} + E_{int} + E_{si} + E_{rw} + E_{damp} + E_{hg} = E_{kin}^{0} + E_{int}^{0} + W_{ext} \qquad (3.9)$$

where;

E_{kin} = Current kinetic energy

E_{int} = Current internal energy

E_{si} = Current sliding interface energy

E_{rw} = Current rigid wall energy

E_{damp} = Current damping energy

E_{hg} = Current hourglass energy

E_{kin}^{0} = Initial kinetic energy

E_{int}^{0} = Initial internal energy

W_{ext} = External work

Among those parameters internal energy is the mainly dealt component. In the above equation, Internal energy includes elastic strain energy and work done in permanent deformation. Thus in the model, *DATABASE_GLSTAT is activated where the internal energy data is printed.

3.2. Optimization study

In the numerical optimization study, two different strategies were followed. Firstly, the total thickness of the sandwich plate was kept constant while the thickness of the foam core was varied from 0.9 to 8.1 cm in order to understand at what thickness range the foam core becomes effective. Once the effective thickness range is defined the study was continued. Secondly, the blast responses of sandwich panels assorted with different face materials were further investigated and the results were compared with those of the corresponding equal-weight monolithic layers.

In order to find out the effective foam thickness for constant sandwich structure thickness, as can be seen from Table 3.2, core thickness was varied in 9 steps starting from 0.9 cm to 8.1 cm.

Table 3.2. Optimization History

ITERATION	CORE DEPTH (cm)	DOWN FACE (cm)	UP FACE (cm)
A	0.9	4.05	4.05
B	1.8	3.6	3.6
C	2.7	3.15	3.15
D	3.6	2.70	2.70
E	4.5	2.25	2.25
F	5.4	1.80	1.80
G	6.3	1.35	1.35
H	7.2	0.9	0.9
I	8.1	0.35	0.35

CHAPTER 4

RESULTS

4.1. Experimental Results

4.1.1. Testing of Glass-fiber Reinforced Polyester Polymer Matrix Composite

4.1.1.1. High Strain Rate Test

Typical SHPB strain readings of a tested composite sample, incident and transmitted readings are shown in Figure 4.1. The variation of the stress and strain rate with the strain for a 0/90 glass-fiber/polyester composite tested in SHPB is shown in Figure 4.2. It is noted in that figure that the strain rate is not constant throughout the SHPB test; therefore, an average strain rate was calculated until about the failure strain. The failure strain of the composite is taken as the strain corresponds to the maximum stress in Figure 4.2. After the maximum stress, the sample fails at ~45 degrees to the loading axis at strain of 3%.

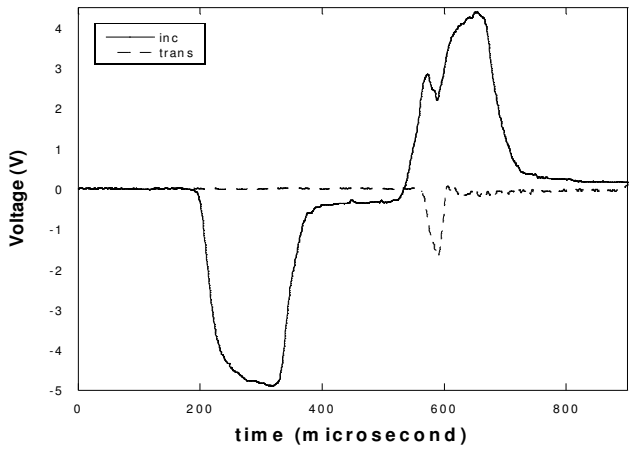

Figure 4.1. Typical SHPB strain gages readings as function of time for the tested composites.

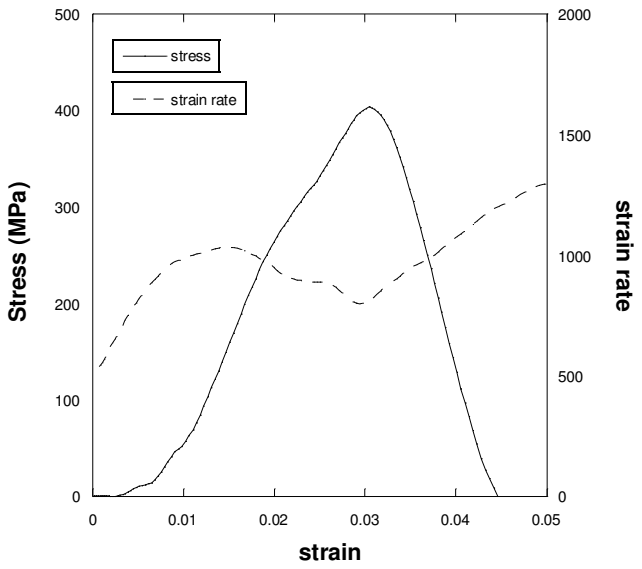

Figure 4.2. Stress/strain and strain rate/strain behavior of 0/90 glass-fiber/polyester composite tested in SHPB.

Figures 4.3 (a-c) shows sequentially stress/strain and strain rate/strain curves +45/-45 glass fiber/polyester composite samples tested through x-, y- and z-directions. The composite shows similar compression behavior through x and y directions, while the compression strength is higher when tested through z-direction, showing a strong anisotropic mechanical response. The compressive strength of the composite tested through x and y-directions varies between 150 and 200 MPa, while through z-direction it increases to 500 MPa. The composite also shows higher failure strains through the z-direction.

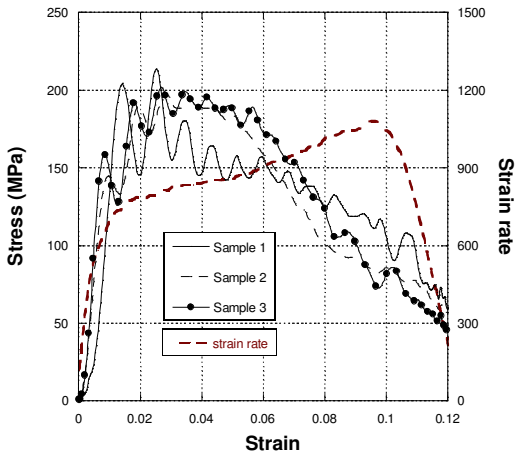

(a)

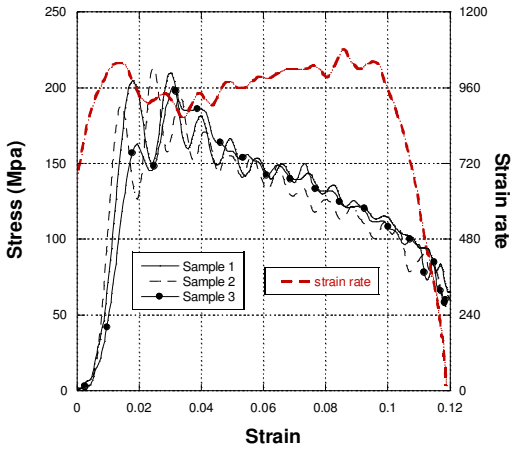

(b)

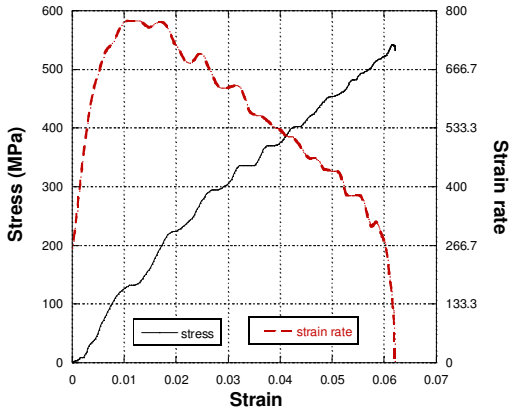

(c)

Figure 4.3. Stress/strain and strain rate/strain behavior of +45/-45 glass-fiber/polyester composite tested in SHPB through (a) x-direction., (b) y-direction and (c) z-direction.

Figures 4.4(a-c) show sequentially stress/strain and strain rate/strain curves 0/90/45/-45 glass fiber/polyester composite samples tested through x-, y- and z-directions. The composite again shows similar compression behavior through x and y directions, while it shows a higher compression when tested through z-direction. The compressive strength of the composite in the x and y-directions varies between 320 and 400 MPa, while through z-direction it is above 500 MPa. Similar to +45/-45 glass-fiber/polyester composite samples, 0/90/45/-45 glass fiber/polyester composite samples show higher failure strains through the z-direction.

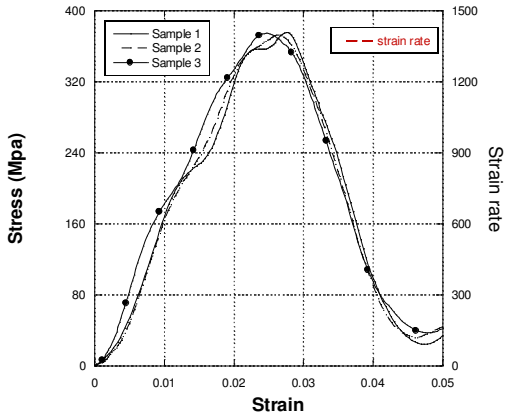

(a)

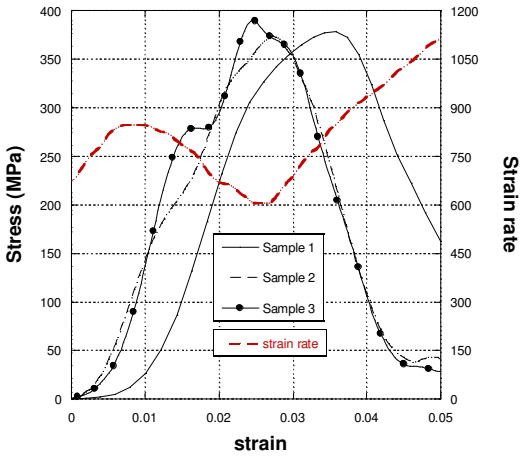

(b)

Figure 4.4. Stress/strain and strain rate/strain behavior of 0/90/45/-45 glass-fiber/polyester composite tested in SHPB through (a) x-direction., (b) y-direction and (c) z-direction.

(cont. on next page)

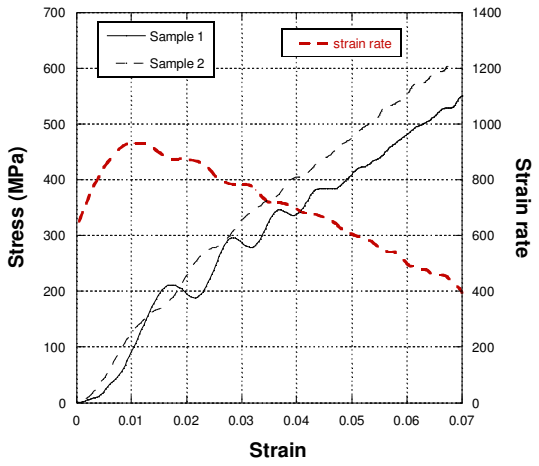

(c)

Figure 4.4. (cont.)Stress/strain and strain rate/strain behavior of 0/90/45/-45 glass-fiber/polyester composite tested in SHPB through (a) x-direction., (b) y-direction and (c) z-direction.

Figures 4.5(a-c) show sequentially stress/strain and strain rate/strain curves 0/90glass fiber/polyester composite samples tested through x-, y- and z-directions. In opposite to previously tested composite samples, 0/90glass fiber/polyester composite samples show similar compressive strength values, varying between 350 and 400 MPa, through x, y and z-directions. However, through z-direction, the composite samples show higher failure strains as seen Figure 4.5(c).

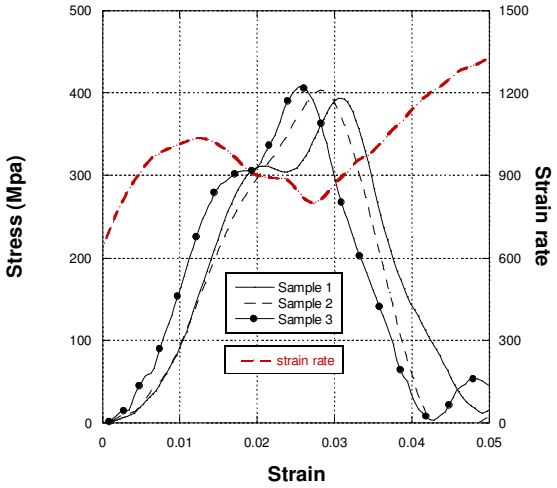

(a)

Figure 4.5. Stress/strain and strain rate/strain behavior of 0/90 glass-fiber polyester composite tested in SHPB through (a) x-direction., (b) y-direction and (c) z-direction.

(cont. on next page)

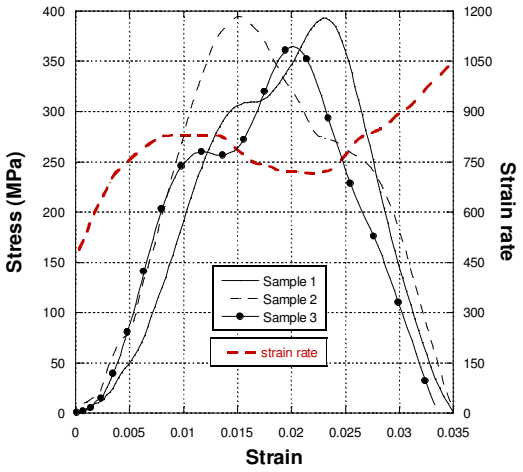

(b)

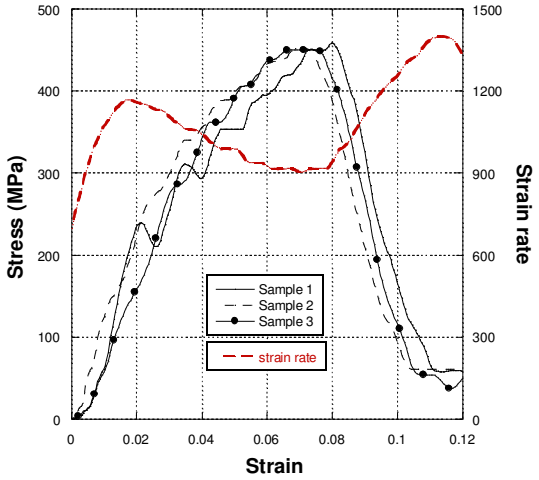

(c)

Figure 4.5. (cont.) Stress/strain and strain rate/strain behavior of 0/90 glass-fiber polyester composite tested in SHPB through (a) x-direction., (b) y-direction and (c) z-direction.

4.1.1.2. Quasi-static Test

The quasi-static compression testing of prepared composite samples were carried out using SHIMADZU mechanical testing device with cross head speed of 1 mm/s. Compression tests results were digitally recorded as load vs. displacement data, which were then converted into nominal stress vs. strain data.

Figures 4.6(a-c) show sequentially stress/strain curves 0/90 glass fiber/polyester composite samples tested through x-, y- and z-directions. The composite shows similar compression behavior through x and y directions, while the compression strength is higher when tested through z-direction, showing a strong anisotropic mechanical response The compressive strength of the composite tested through x and y-directions varies between 275 and 325 MPa, through x, y and z-directions. However, through z-direction, the composite samples show higher failure strains as seen Figure 4.6(c).

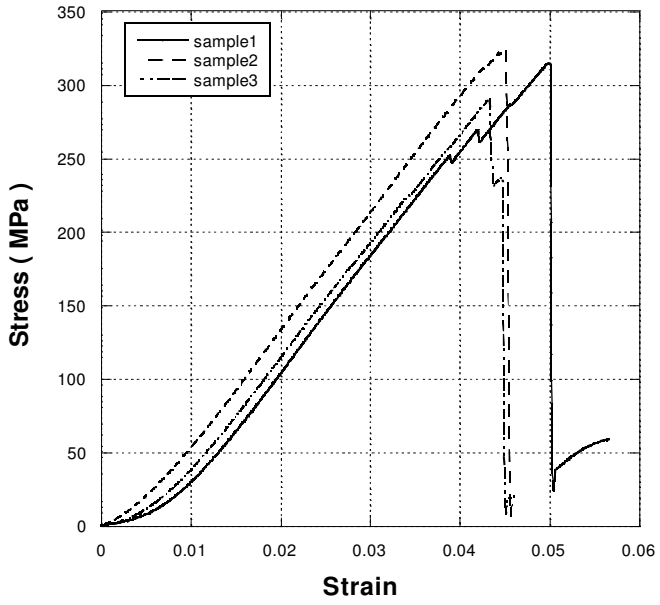

(a)

Figure 4.6. Stress-strain behavior of 0/90 glass-fiber polyester composite tested in mechanical testing device through (a) x-direction., (b) y-direction and (c) z-direction.

(cont. on next page)

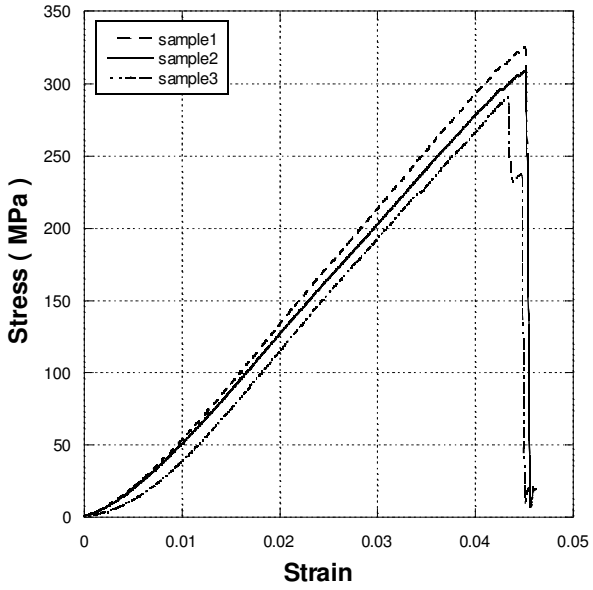

(b)

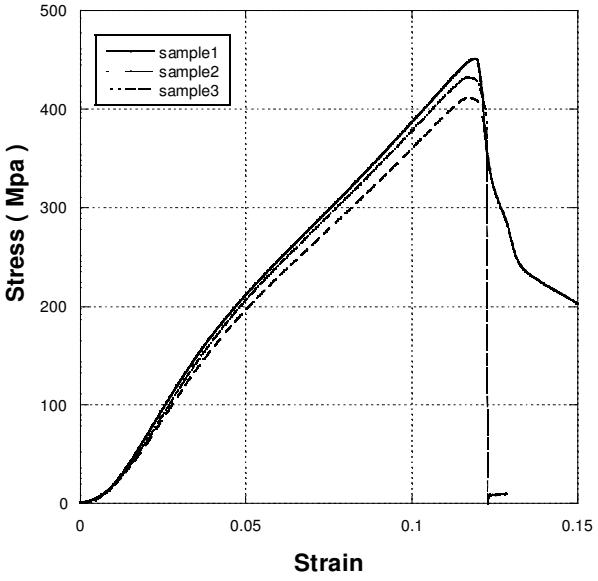

(c)

Figure 4.6. (cont.) Stress-strain behavior of 0/90 glass-fiber polyester composite tested in mechanical testing device through (a) x-direction., (b) y-direction and (c) z-direction.

Figures 4.7 (a-c) show sequentially stress/strain curves 45/-45 glass fiber/polyester composite samples tested through x-, y- and z-directions. The composite again shows similar compression behavior through x and y directions, while it shows a higher

compression when tested through z-direction. The compressive strength of the composite in the x and y-directions varies between 110 and 140 MPa, while through z-direction it is above 570 MPa. Similar to 0/90 glass-fiber/polyester composite samples, +45/-45 glass fiber/polyester composite samples show higher failure strains through the z-direction.

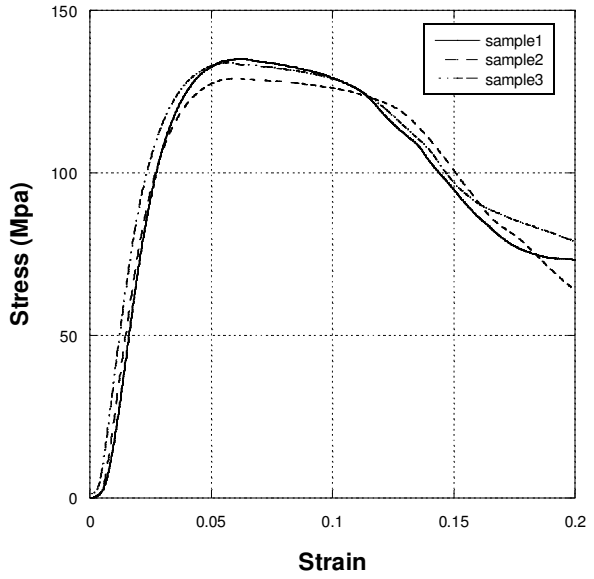

(a)

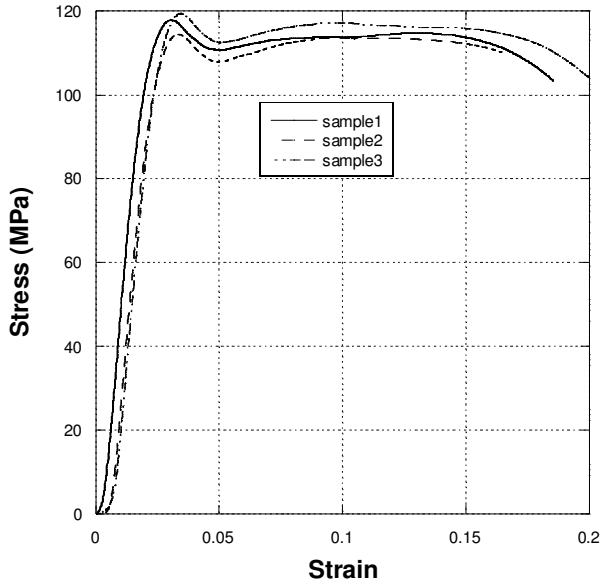

(b)

Figure 4.7. Stress-strain behavior of 45/-45 glass-fiber polyester composite tested in mechanical testing device through (a) x-direction., (b) y-direction and (c) z-direction.

(cont. on next page)

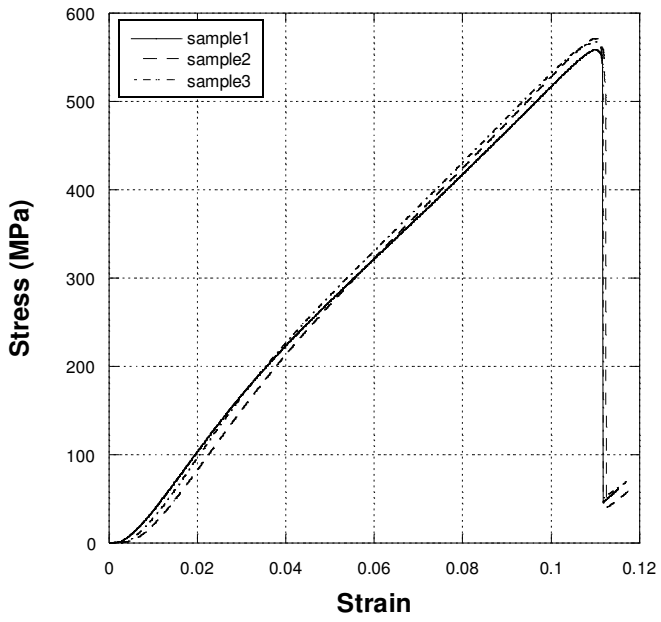

(c)

Figure 4.7. (cont.)Stress-strain behavior of 45/-45 glass-fiber polyester composite tested in mechanical testing device through (a) x-direction., (b) y-direction and (c) z-direction.

Figures 4.8(a-c) show sequentially stress/strain curves 0/90/45/-45 glass fiber/polyester composite samples tested through x-, y- and z-directions. 0/90/45/-45 glass fiber/polyester composite samples show similar compressive strength values, varying between 300 and 350 MPa, through x, y and is about 500 MPa z-directions. However, through z-direction, the composite samples show same failure strains and maximum stresses for 45/-45 and 0/90/45/-45 as seen Figure 4.7(c)-4.8(c).

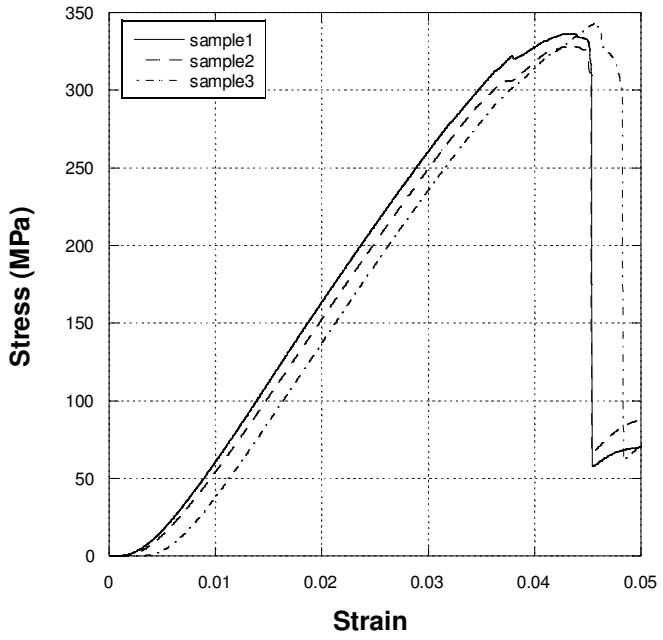

(a)

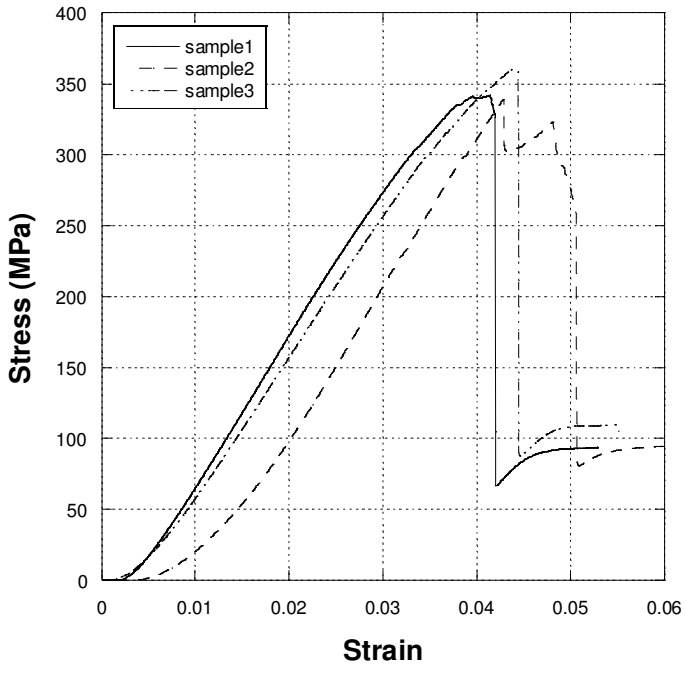

(b)

Figure 4.8. Stress-strain behavior of 0/90/45/-45 glass-fiber polyester composite tested in mechanical testing device through (a) x-direction., (b) y-direction and (c) z-direction.

(cont. in next page)

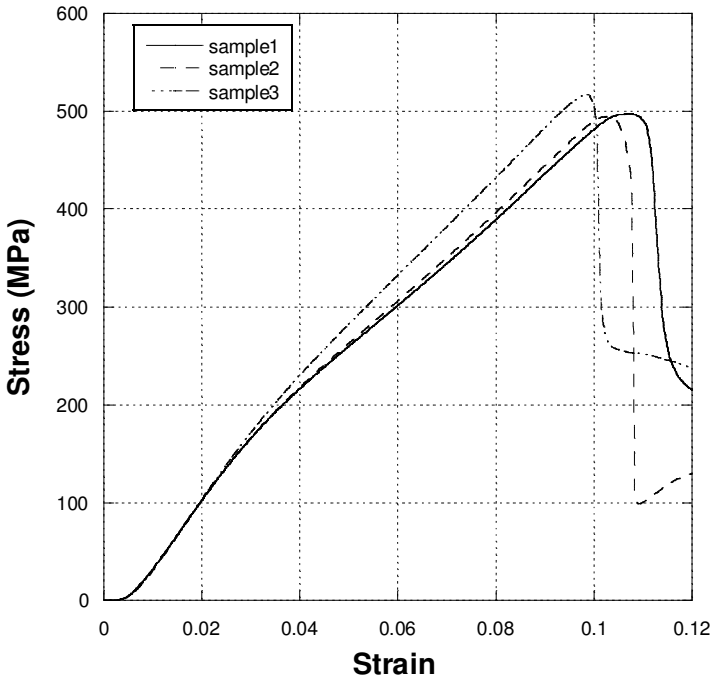

(c)

Figure 4.8. (cont.) Stress-strain behavior of 0/90/45/-45 glass-fiber polyester composite tested in mechanical testing device through (a) x-direction., (b) y-direction and (c) z-direction.

Briefly calculated mechanical properties of composites are given in Table 4.1.

Table 4.1. Mechanical properties of composite samples

MECHANICAL PROPERTIES OF COMPOSITES		0/90			45/-45			0/90/45/-45		
		x	y	z	x	y	z	x	y	z
High Strain Rate Test	Elastic Module (GPa)	36.386	36.163	9.5331	23.065	21.868	7.526	23.812	21.911	7.441
	Failure Strength (MPa)	399.54	383.95	450	168.33	187.586	541.66	374.5	380.63	575.3
	Failure Strain	0.028	0.02	0.072	0.01	0.017	0.061	0.025	0.027	0.069
Quasi static Test	Elastic Module (GPa)	7.8825	7.9675	3.846	5.137	6.41	5.402	9.821	10.074	4.43
	Yield Strength (MPa)	315.97	308.32	431.92	132.5	117.27	565	336,28	350.72	497
	Failure Strain	0.05	0.0442	0.117	0.057	0.03	0.11	0.037	0.04	0.105

4.1.2. Testing of Aluminum Foam

Aluminum foams were tested only quasi-statically. Because in material model 26 (MAT_HONEYCOMB), quasi-static mechanical properties were used.

4.1.2.1. Quasi-static Test

In axial compression loading, stress-strain behavior of metallic foams has been fitted with the various kinds of equations based on usually simple models such as the unit cell model construction of the beams representing the cell edges in open-cell foam. The models used for the constutive equations of metal foams are generally based on the scaling equations. The mechanical properties scale with relative density and the

mechanical properties of the metal from which the foam is made of. Different models are also used for open and closed-cell foams. However, the models developed for open-cell models can also be applied to closed-cell foams as relatively high ratio of metal found in the cell edges of closed-cell foams, making them very much similar to open cell foams. The stress-strain relation of Al foams used in this thesis is fitted with the following empirical equation,

$$\sigma = \sigma_{pl}\left[\frac{1}{D}\left(\frac{e_D}{e_D - \mathrm{e}}\right)^m\right] \tag{4.1}$$

In Equation 4.1, σ_{pl}, e and e_D are the plateau stress, strain and densification strain, respectively. D and m are constants. The densification strain is given as,

$$\varepsilon_D = 1 - 1.4\rho \tag{4.2}$$

where, ρ is the relative density of the foam (foam density/foam metal bulk density). The plateau stress is calculated using the following equation developed for closed cell foams,

$$\frac{\sigma_{pl}}{\sigma_{ys}} = 0.3(\phi\rho)^{3/2} + (1-\phi)\rho \tag{4.3}$$

where, σ_{ys} and ϕ are the yield strength of aluminum and the ratio of the metal found in the cell edges. The value of ϕ is calculated using the following relation

$$\phi = 1 - \frac{3t(l-2w_p)^2 + 6t\sqrt{3}(l-(2/\sqrt{3})w_p)^2}{11.31\ l^3\rho} \tag{4.4}$$

where l, w_p, and t are the cell wall length, the thickness of the cell edge and the thickness of cell wall (Figure 4.9). For aluminum foams tested, the following values of the parameters are found microscopically: t=0.05 mm, w_p=12.5 mm and l= 25 mm. The value of ϕ using these values, is calculated 0.95. A relatively high value of ϕ shows a relatively high metal concentration in the cell edges. Then, Equation 4.1 can be arranged as,

$$\sigma = \sigma_{ys}(0.3[0.95\rho]^{3/2} + 0.05\rho)\left[\frac{1}{D}(\frac{e_D}{e_D - e})^m\right] \quad (4.5)$$

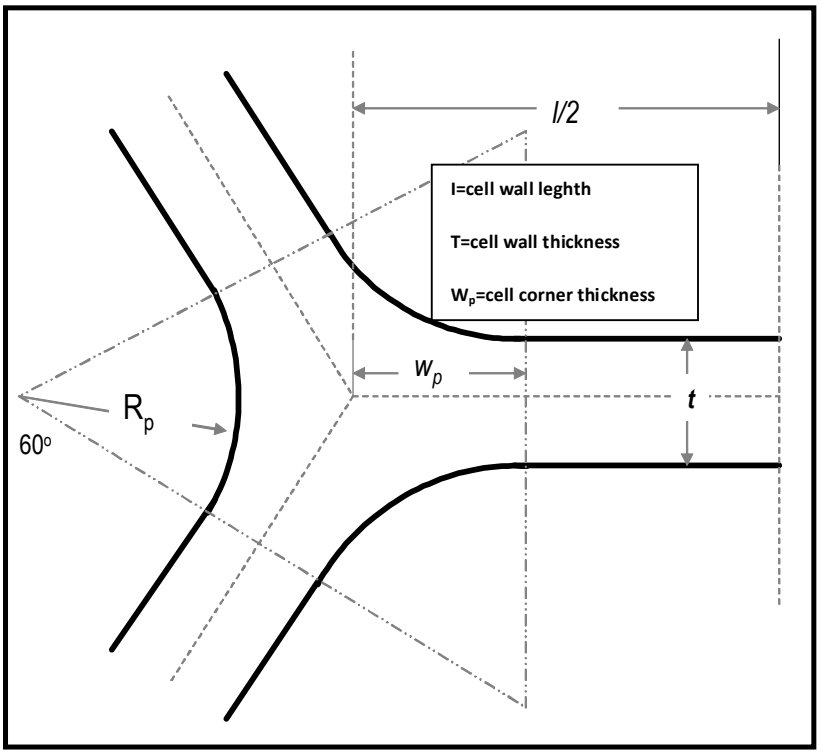

Figure 4.9. Cell edge and cell wall

The yield strength of aluminum was determined by the hardness test as 104 MPa. The experimental stress-strain curves of aluminum foams of varying relative are fitted with Equation 4.5 and the results are shown in Figure 4.10. The fitting gives the values of D and m as 0.8 and 1, respectively.

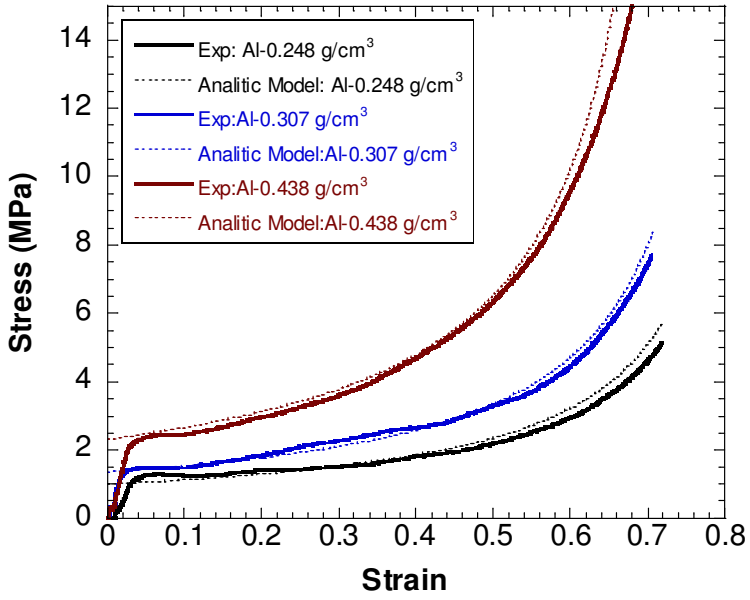

Figure 4.10. Experimental and estimated stress-strain curves of aluminum foam of various relative densities.

4.2. Finite Element Results and Discussion

4.2.1. Sandwich Structure Finite Element Model Results and Discussions

In previous section, a complete analysis of the results of glass fiber reinforced polyester matrix composites' SHPB experiments and quasi-static behavior of aluminum foams were done and given. Then finite element analysis of sandwich structures were done by using founded material constants by changing parameters (Core thickness, face thickness and face material). Now in this section, results of numerical analysis will be given graphically and numerically, discussed in greater detail and compared with previous study's results.

A typical series of deformation for an aluminum core sandwich plate (6.3 cm aluminum foam core and aluminum faces) is shown in Figure 4.11. The core is completely deformed at 200 microseconds and at this time; the total energy and internal energy become steady state.

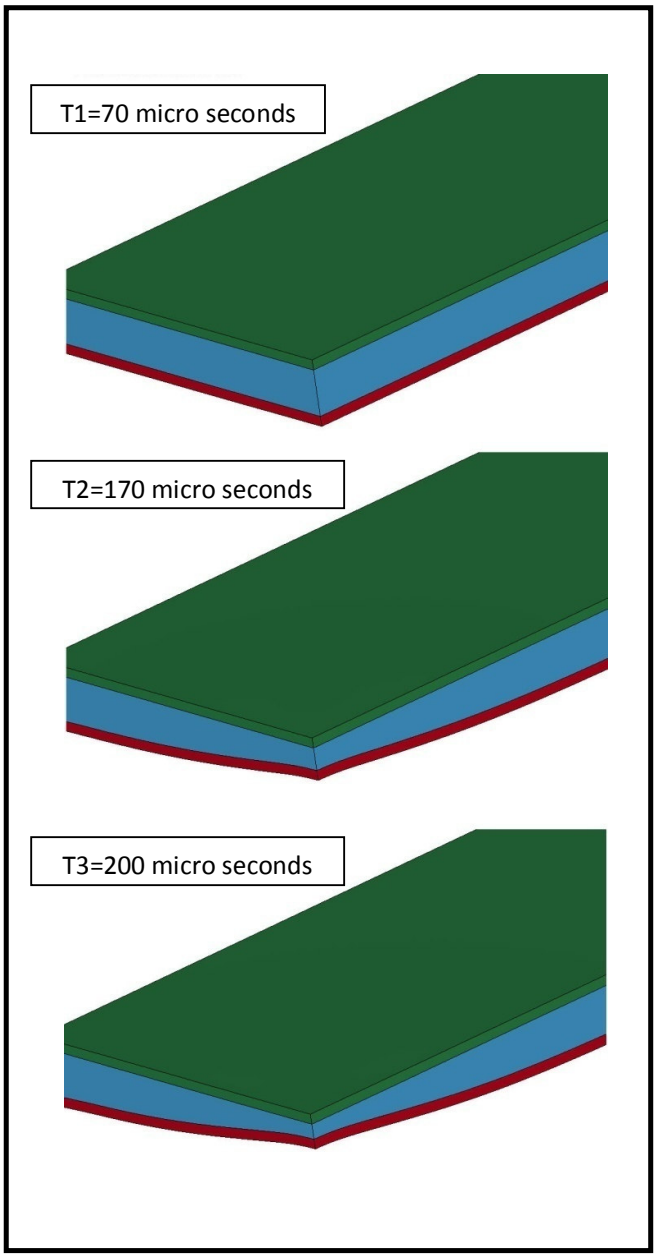

Figure 4.11 Deformation history of aluminum foam core sandwich plate exposed to blast loading

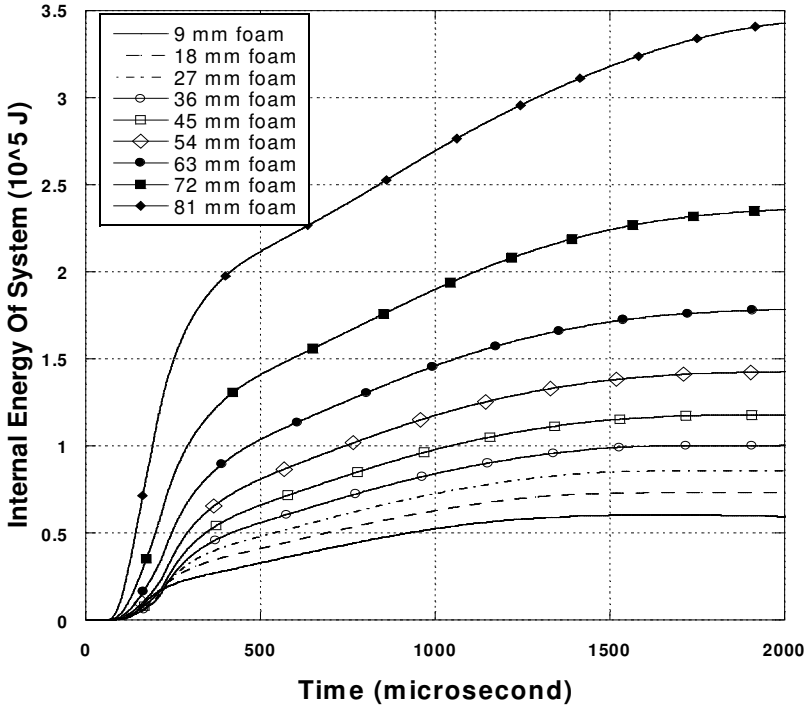

Figure 4.12. Internal energy of the sandwich structure as function time, for indicated core thicknesses.

Internal energy of the sandwich structure as a function of time for different core thicknesses is shown in Figure 4.12. As the core thickness increases, the total internal energy of the panel increases as the energy absorption capability of the foam layer increases. This figure clearly shows that the sandwich structure becomes more effective as the core thickness increases. This result is also in accord with the results of previous studies by Radford et al (D.D. Radford 2005) and Hutchinson (John W. Hutchinson 2003).

The effectiveness is however limited with both front and back face plate thicknesses. Increasing the foam core thickness too much significantly decreases the thicknesses of front and back face plate as the total thickness of the sandwich plate was kept constant in this study. Numerical simulation results also show that the permanent deflection increases as the thickness of the foam core increases as depicted in Figure 4.13.

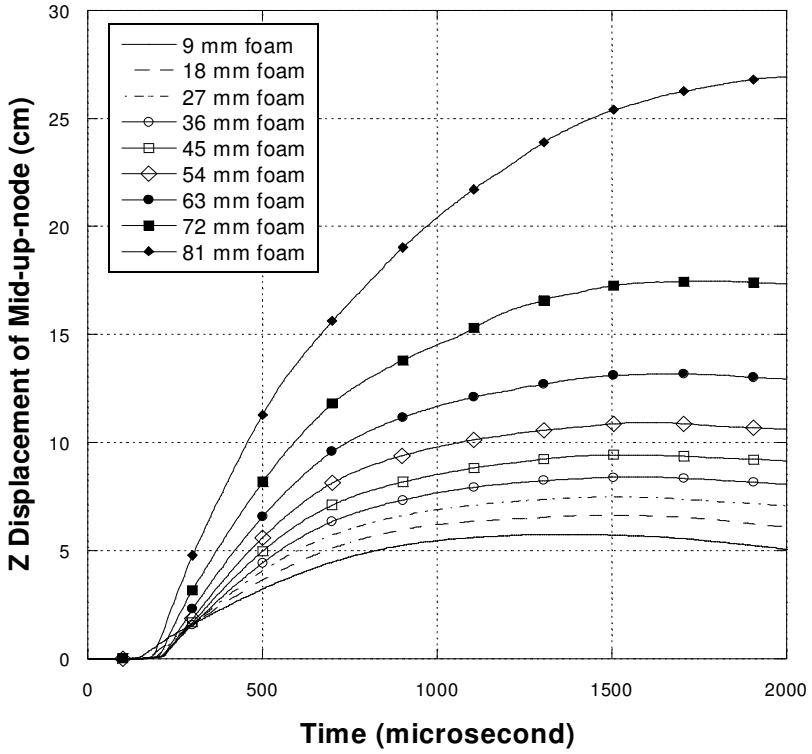

Figure 4.13. Deflection of Plate's center as a function of time, for indicated core thicknesses.

During the blast loading of sandwich structures, faces resist to the bending moment as longitudinal compressive and tensile stresses while the foam core carries the transverse shear force. Faces start yielding when equivalent stress exceeds the yield stress of the material and if the loading is further continued finally the material ruptures. Faces can also wrinkle when the stress values exceed the local instability stresses. Numerical simulations reveal that 72 mm and thicker cores cause significantly higher deflections and catastrophic failure of the whole structure. Therefore; 63 mm and 72 mm thick foam cores were chosen for the rest of the numerical study. These two thickness values can both give the full advantage of absorbing significant amount of energy while without significantly decreasing the strength of the overall structure.

Figure 4.14 shows the acceleration history of each component of the sandwich plate (6.3 cm foam core). As shown in this figure, the front face and the core accelerate

quickly as the blast wave propagates in the plate. The foam core significantly delays the wave passage between the front and back face. It is also noted in the same figure that the back face acceleration is slower than the front face for all the time values. There is about 66.8 % reduction in peak acceleration in the back face as compared with the front face. Due to higher acceleration the deformation of the front plate is much faster than that of back panel. Moreover, the back face experiences no negative accelaration during the loading history as opposite to front face and foam core. The front face always experiences the highest acceleration levels as the foam core thickness incerase (Figure 4.15). The increase in foam core thickness is however less effective in increasing the peak acceleration of the back plate when compared with front plate.

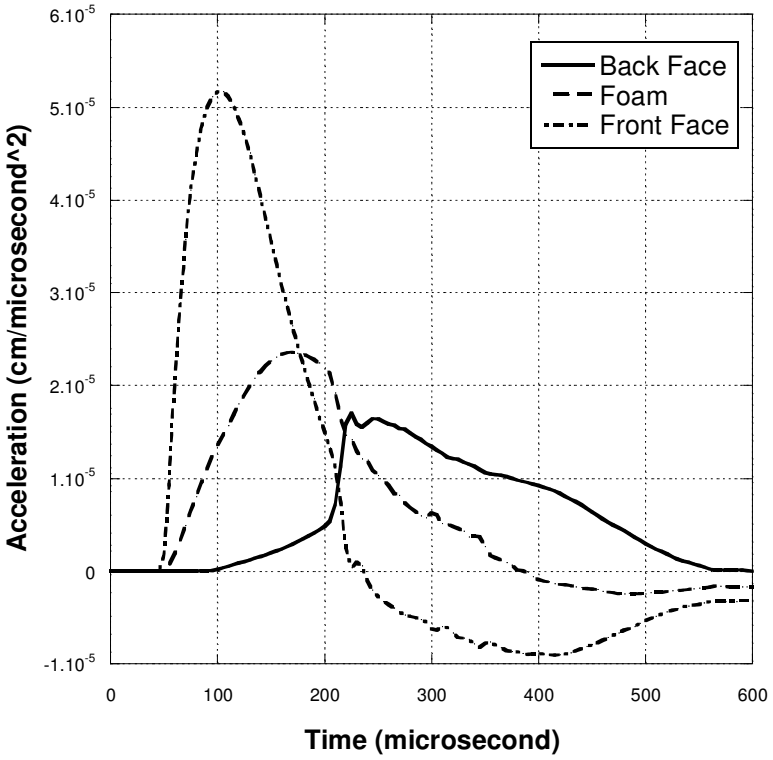

Figure 4.14. Typical Acceleration History of Sandwich plate

Figure 4.16 shows that the delay time (the time diffeneces between the acceleration starting points of front and back plate) almost linearly increases with the

foam thickness for a constant foam density. This implies that increasing foam core thickness up to a certain level can significantly alters the blast response of the panel.

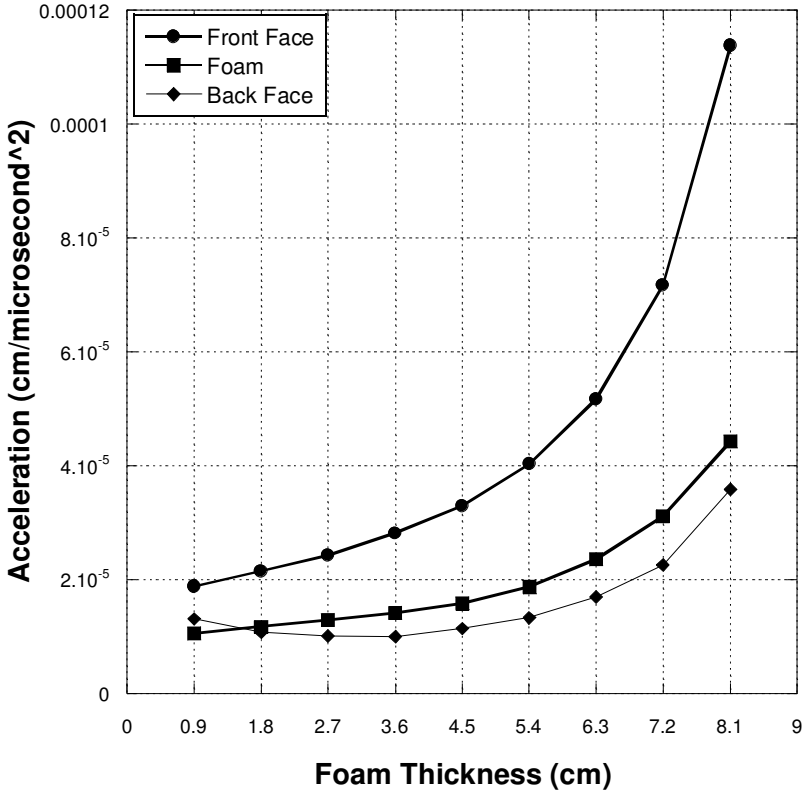

Figure 4.15. Comparison of peak acceleration of each component for different foam core thicknesses

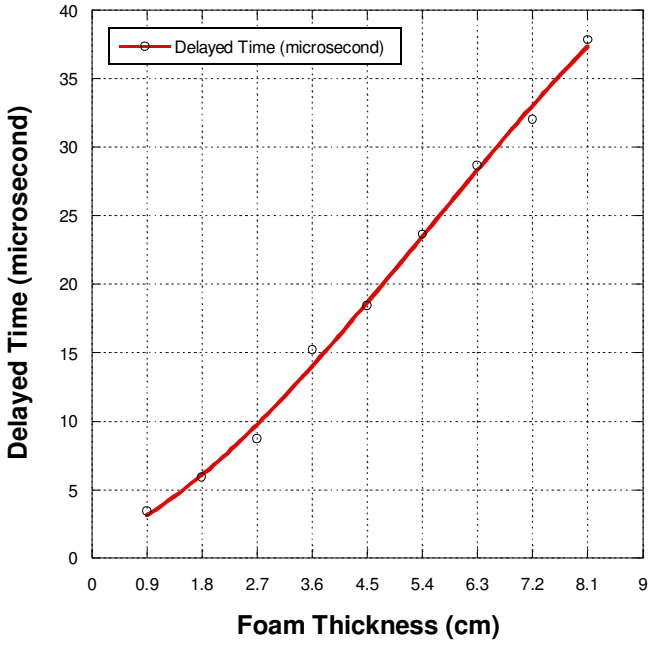

Figure 4.16. Delayed time of back face acceleration as a function of core thicknesses

The blast performance Al/Al-foam/Al sandwich structure with the optimized face and core thickness is compared with that of monolithic Al plate having the same weight with the sandwich plate. The geometric dimensions of the sandwich and monolithic plates are tabulated in Table 4.2. The corresponding monolithic plates thicknesses of 6.3 cm and 7.2 cm thick foam sandwich plates based on equal mass are 3.57 and 2.79 cm, respectively.

Table 4.2. The geometric dimensions of the plates

	CORE DEPTH (cm)	FACES DEPTH (cm)	BULK DEPTH (cm)
1	6.3	2.7	3.5767
2	7.2	1.8	2.79779

Figure 4.17 shows the internal energy histories of the sandwich and monolithic plates for 63 mm and 72 mm thick foam core sandwich and corresponding monolithic plates. It is noted in Figure 4.17 the blast wave diminishes after 2000 microseconds. Foam cored sandwich plates show higher internal energies as compared with monolithic plates. The rate of internal energy increase particularly in the initial region is also much higher in foam core sandwich plates. This is attributed to the constant stress deformation of the foam core in the plateau region.

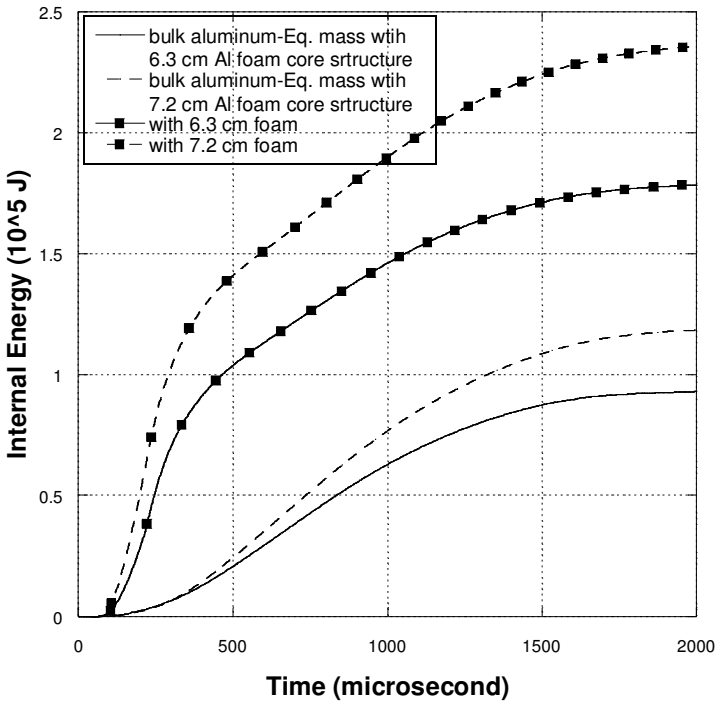

Figure 4.17. Comparison of Internal energy of sandwich structures with aluminum faces and monolithic plate

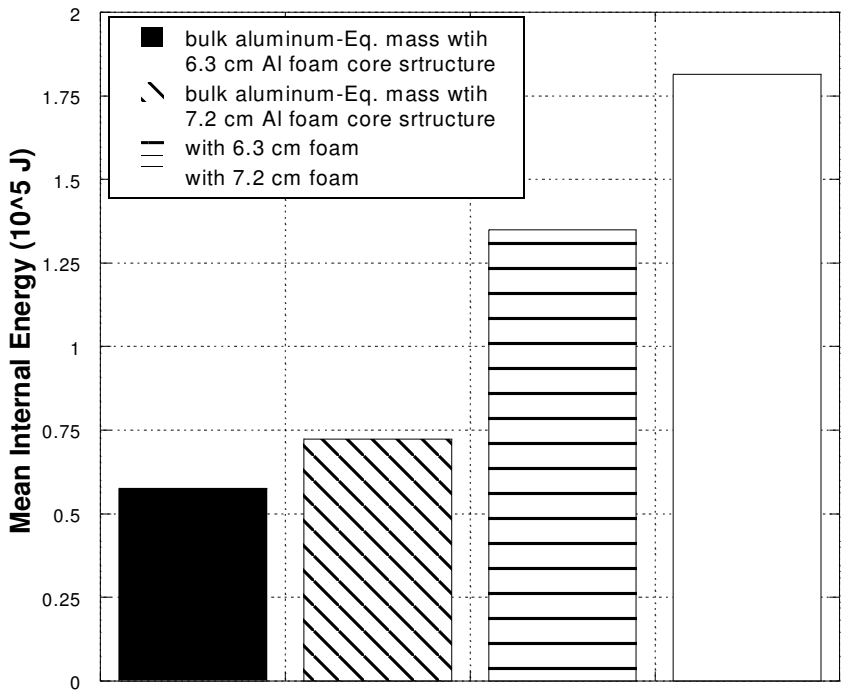

Figure 4.18. Internal energy change as percentage between sandwich structure with aluminum foam and equal-mass bulk aluminum

The average internal energy values of sandwich plates are compared with those of the monolithic plates in Figure 4.18. The average internal energy is calculated by integration internal energy with respect time and dividing the integration by the total time. The absorbed energy increases 136 % and 151.53 % for 63 mm and 72 mm aluminum foam core sandwich plates compared to equal-mass monolithic plates.

In order to compare the blast response of the sandwich plates with monolithic plates of equal masses, steel /Al-foam/steel sandwich plates are also simulated. The geometric dimensions of the plates are listed in Table 4.3.

Table 4.3. The geometric dimensions of the plates

	CORE DEPTH (cm)	FACES DEPTH (cm)	BULK DEPTH (cm)
1	6.3	0.915	1.2673
2	7.2	0.61	1.012

Figure 4.19 shows the internal energy histories of the sandwich and monolithic plates for 63 mm and 72 mm thick foam core sandwich and coresponding monolithic plates. The variations of mean internal energies are also calculated and are shown in Figure 4.20.

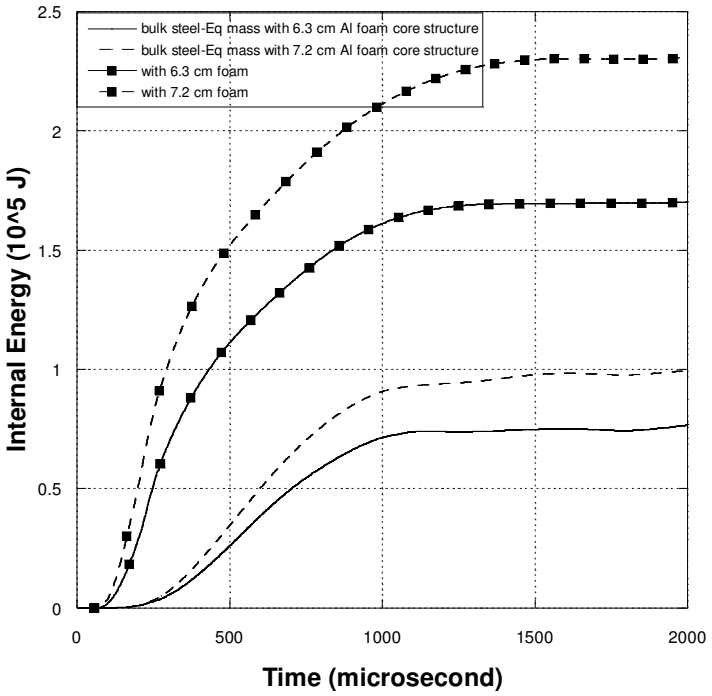

Figure 4.19. Comparison of Internal energy of sandwich structures with steel faces and monolithic plate

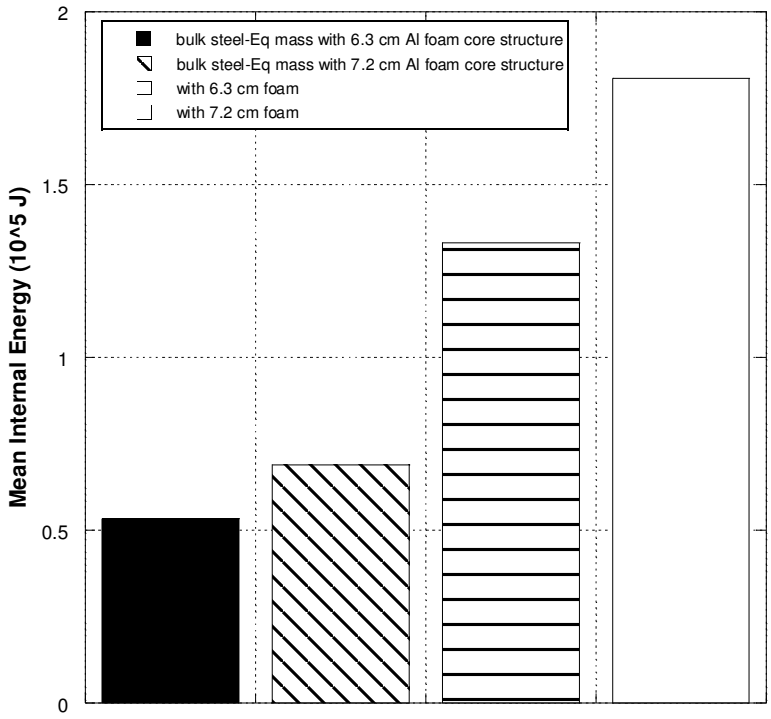

Figure 4.20. Internal energy change as percentage between sandwich structure with aluminum foam-steel faces and eq-mass bulk steel

The sandwich structure increases, as compared to equal-mass monolithic plates, the mean internal energy by %151 and %160 for 63 mm and 72 mm aluminum foam core sandwich plates with steel faces, respectively,

After giving results of this two study, for comparing the blast response of the sandwich plates with monolithic plates of equal areal mass, it is clearly seen that energy absorbing capability of sandwich structures is about 2 times higher than monolithic plates. In the litearature, Radford et al. (2005) showed same result that a higher shock resistance of aluminum foam core sandwich panels than plate structures when a projectile impacts a sandwich panel.

Similar numerical analyzes were repeated for 6.3 cm foam cored sandwich structures of Aluminum 5083-H112, AISI 4340 steel, Ti6Al4V and their combinations. The geometric dimensions of the plates are listed in Table 4.4.

Table 4.4. The geometric dimensions of the plates

Face material	**Al/Al Face (cm)**	**Steel/Steel Face (cm)**	**Down Steel/Up Al Face (cm)**	**Down Al/Up Steel Face (cm)**
Thickness of faces (cm)	1.35-1.35	0.4575-0.4575	0.4575-1.35	1.35-0.4575
Face material	**Ti/Ti Face (cm)**	**Ti/Al Face (cm)**	**Ti/Steel Face (cm)**	**Composite /Composite Face**
Thickness of faces (cm)	0.835-0.835	0.835-1.35	0.835-0.4575	2-2

Figure 4.21 shows the internal energy history of the 6.3 cm aluminum core sandwich panels with different faces and combinations. As seen from Figure 4.21, there is no significant difference between face material and internal energy. Due to fact that, another parameter, deflection of plate's center as a function of time, for indicated face material was decided to investigate.

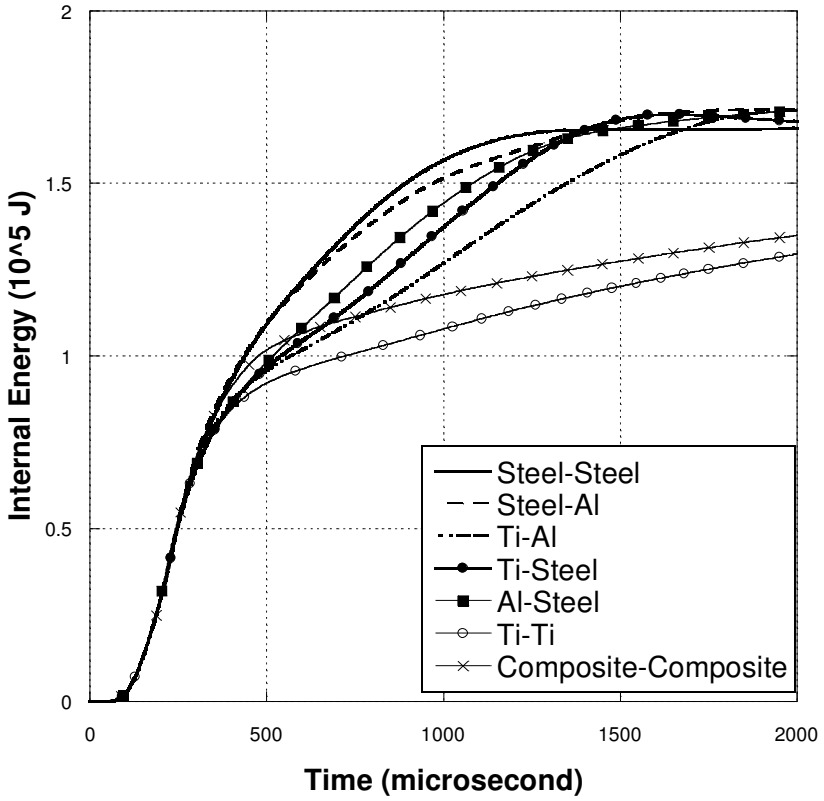

Figure 4.21. Comparison of internal energy of sandwich structures with different faces

The comparison of the deflection of plate's center as a function of time material is shown in Figure 4.22. It is clearly seen in this figure that the face material has a significant effect on the deflection of the plates. Considering the plate deflections, one can conclude that the steel-steel face combination is the best face material combination whereas Ti-Al face combination is the worst.

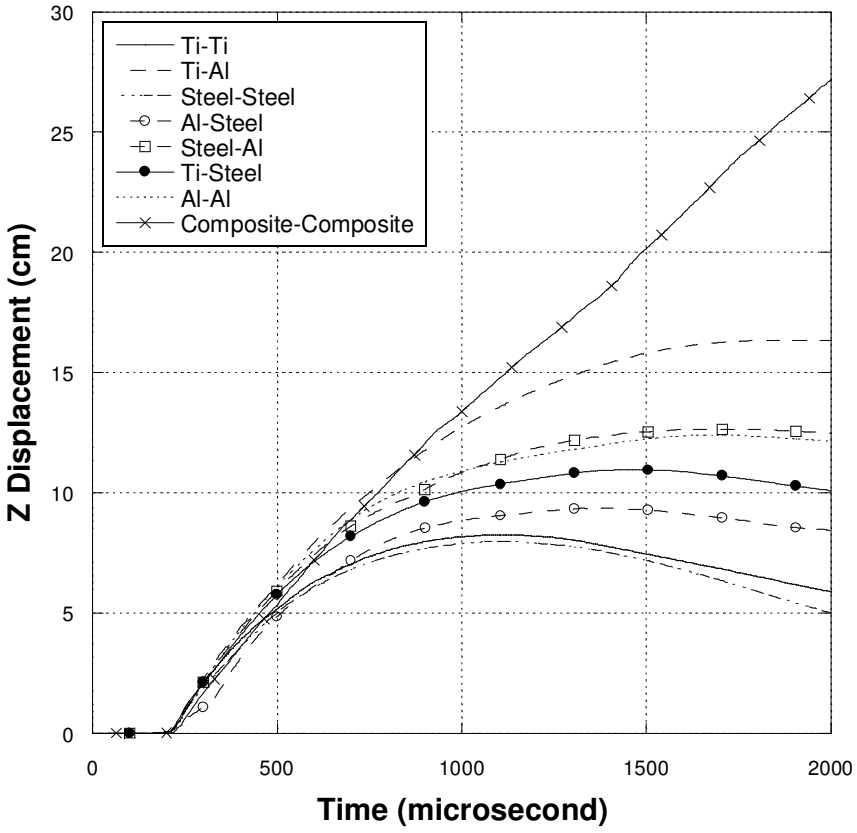

Figure 4.22. Deflection of Plate's center as a function of time, for indicated core thicknesses

4.2.2. E-Glass / Polyester Composite Results and Discussions

In this section, blast response of E-glass/polyester composites with three different lay-ups was investigated, namely 0/90, 45/-45 and 0/45/90/-45. In order to investigate the effect of fiber lay-up, three different composite panels having same thicknesses were subjected to 500 gr TNT explosive load.

Internal energy histories of composite panels corresponding to different fiber lay-ups were given in Figure 4.23

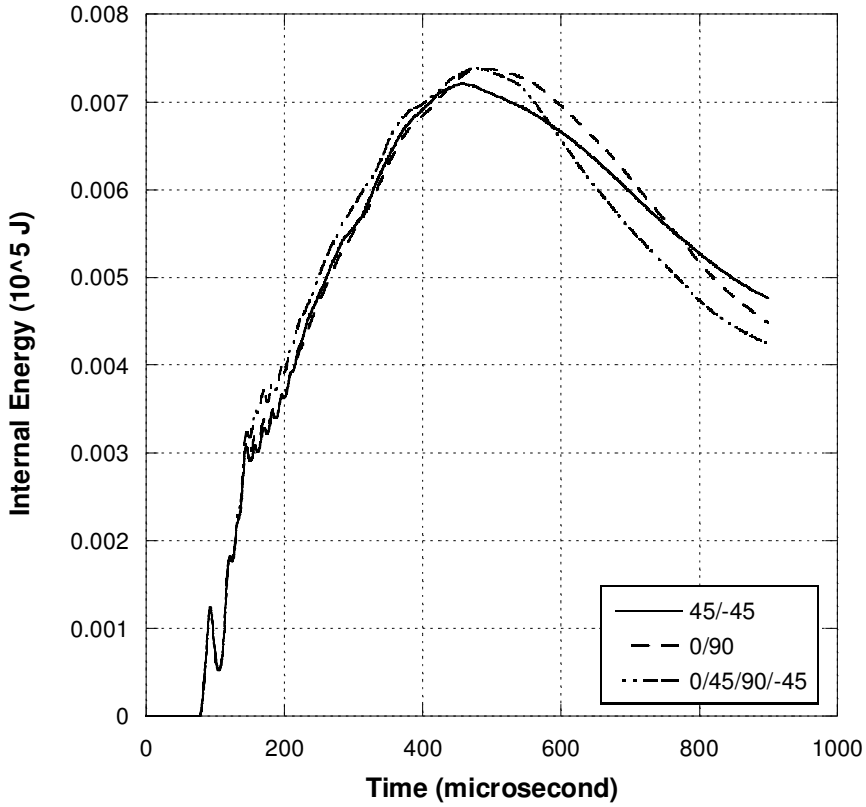

Figure 4.23. Comparison of internal energy of composite panels corresponding to different fiber lay-ups

It is observed that these three plates behaved identically the same up to time 144 microsec. Dishing occurred at time 94 which caused a kink formation in the internal energy history. It is observed that 0/45/90/-45 plate absorbed little more energy than the other two plates from 144 to 430 microseconds.

Figure 4.24 shows that deflection of plate's center as a function of time, for indicated fiber lay-up.

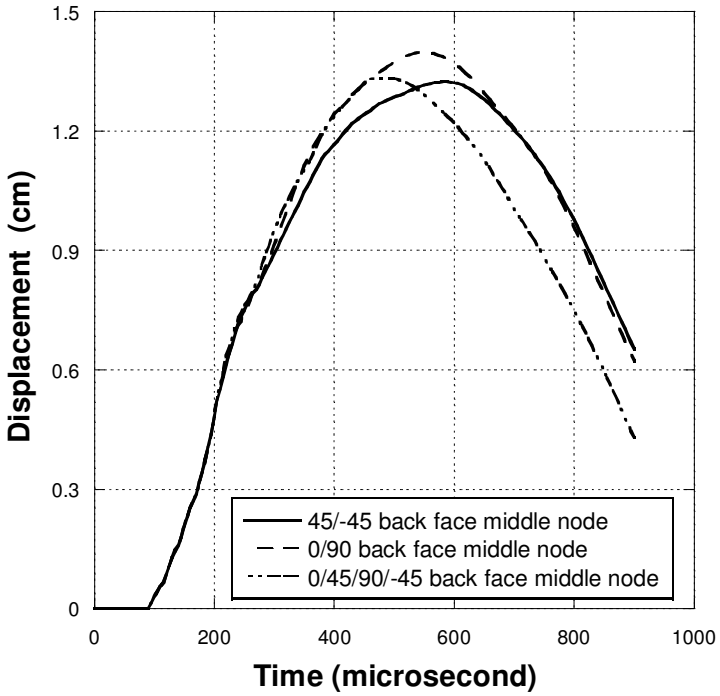

Figure 4.24. Deflection of Plate's center as a function of time, for indicated fiber lay-up

It is noted that the plate having 0/90 lay-up displaced the most while the other two displaced to similar magnitudes of displacement but with time-shift. Up to time 261 microsecond, the displacement rate i.e. velocity remained the same for all the plates. It is seen that the displacement history of +45/-45 plate slightly deviates from the other two from 261 microsecond to the time where peak displacement occurs.

Resultant momentum histories of composite panels corresponding to different fiber lay-ups were given in Figure 4.25.

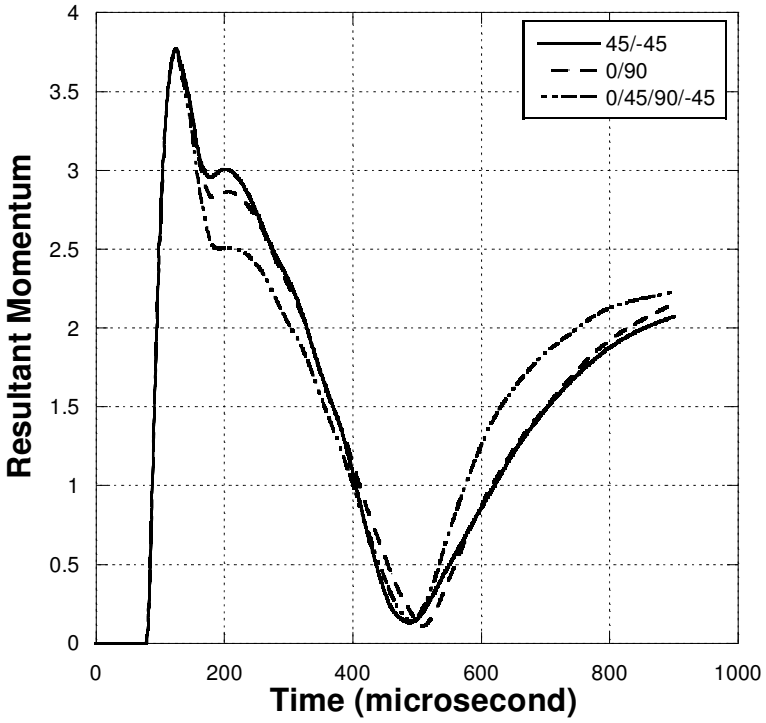

Figure 4.25. Comparison of resultant momentum of composite panels corresponding to different fiber lay-ups

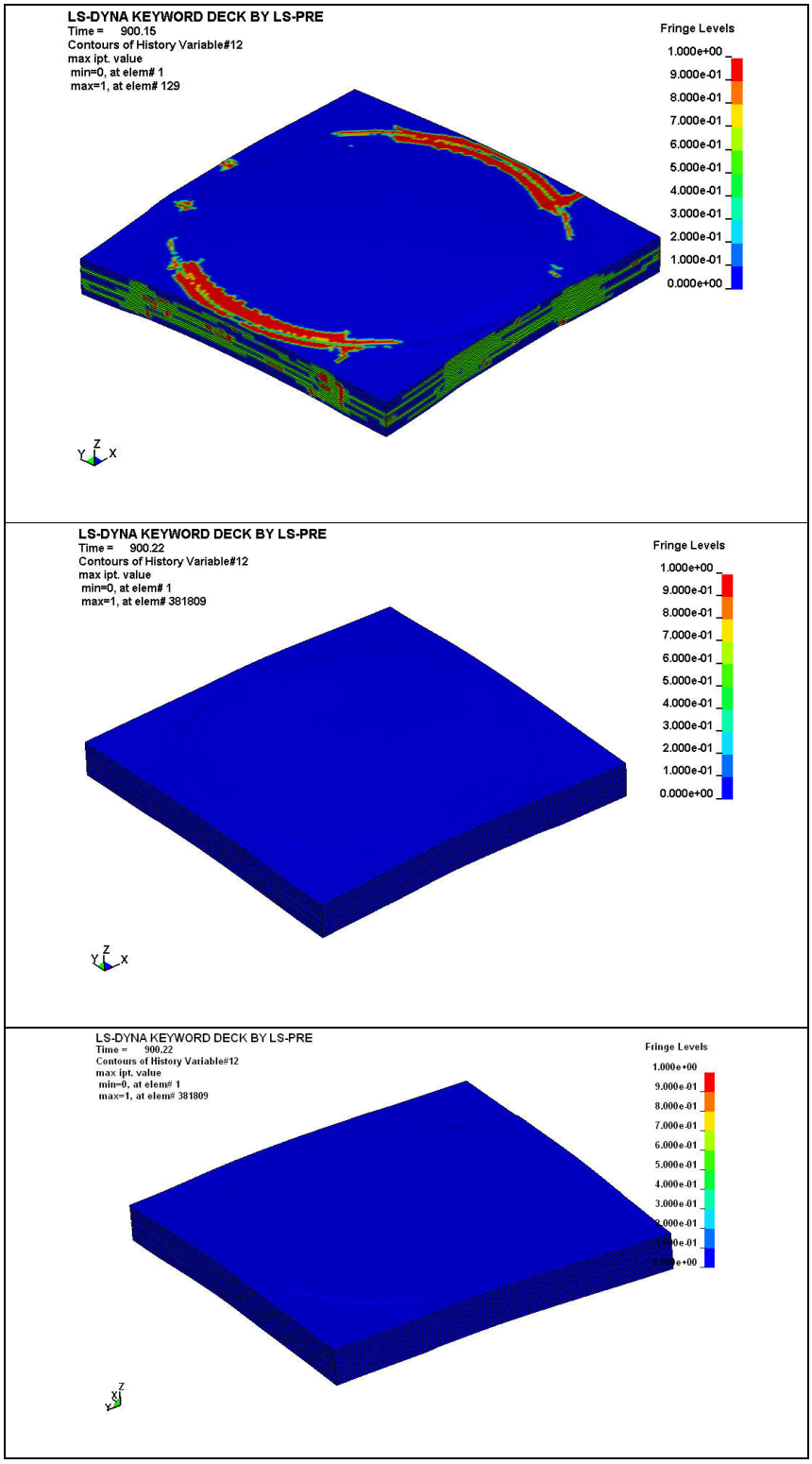

Figure 4.26 Delemination history of 0/90,45/-45 and 0/45/90/-45 lay-ups composite plates

Again, resultant momentum histories of all the plates are exactly the same up to time 125 microsecond. After time 125 microsecond, resultant momentum begin to decrease and showing a minimum value at time 495 microsecond. When the internal energy histories of these three plates are compared, it is seen that 0/90 and 0/45/90-45 plates absorbed the highest and similar magnitudes of internal energy. Since 0/45/90/-45 plate deformed 20 % less as compared to the 0/90 plate and due to delemination history it has less damage, it is concluded that the blast performance of 0/45/90/-45 is the best among these three.

CHAPTER 5

CONCLUSIONS AND SUGGESTIONS FOR FUTURE WORKS

Blast response and energy absorption capability of aluminum foam core sandwich structures E Glass/Polyester composites were investigated by using commercial explicit finite element code LS-DYNA. SHPB tests were done for fiber glass reinforced polyester matrix composites to achieve high strain rate deformation behavior of composites. Experimental and numerical studies revealed the following conclusions;

- Aluminum foam core lightweight sandwich structures have been found to be very effective in energy absorption under blast loading. The results are consistent with the previous studies such as the core thickness increases, the total internal energy of the panel increases, due to the energy absorption capability of the foam layer.

- Sandwich structures absorbed more energies than the bulk materials from %50 to %150 when appropriate combinations of core and face materials are used.

- Numerical simulations showed that 6.3 and 7.2 cm thick foam interlayer are the most efficient foam thicknesses for a 9 cm sandwich plate against 10 kg TNT blast load.

- Another important conclusion is for the same blast threat i.e. 10 kg of TNT, AISI 4340 Steel is the most effective face material.

- 0/45/90/-45 lay-up is most convenient lay-up for E-glass/polyester composite against blast load.

For the future works, achieved results by using finite element analysis can be manufactured and tested experimentally to compare results. The core material can be changed and all optimization can be remade to investigate the blast response.

REFERENCES

A.G. Hanssen, L. E., M. Langseth. 2001. Close-range blast loading of aluminum foam panels. *International Journal of Impcat Engineering* 27: 593-618(26).

Baumeister J. 1996. German Patent 40 18 360 1990; US Patent 5,151,246 1992; Europen Patent EP 0460392A1 1996.

Baumeister J., B. J., Weber M. 1997 . German Patent DE 44 26 627.

Baumeister J., S. H. 1991. German Patent DE 41 01 630 .

C.F. Yen, R. S., and B.A. Cheeseman. 2005. Modeling of shock mitigation sandwich structures for blast protection. *The 3rd First International Conference on Structural Stability and Dynamics.*

Cole, R. H. 1948. Underwater Explosions. *Princeton University Press, NJ.*

D.Boyd, S. 2000. Acceleration of a Plate Subject to Explosive Blast Loading-Trial Results. *Defence science and technology organization.* DSTO-TN-0270.

D.D. Radford, G. J. M., V.S. Deshpande, N.A. Fleck. 2005. The response of clamped sandwich plates with metallic foam cores to simulated blast loading. *International Journal of Solids and Structures.* Volume 43, Issues 7-8, Pages 2243-2259.

Dong Kwan(David) Lee, B. J. O. T. 2004. Energy Absorbing Sandwich Structures Under Blast Loading. *8th International LS-DYNA User Conference.*

F. Zhu, G. L. 2007. A Rewiev of Blast and Impact of Metallic and Sandwich Structures. *EJSE International-Loading and Structures*.

Fleck, N. A. 2006. The impulsive response of sandwich beams: Analytical and numerical investigation of regimes of behavior. *Journal of the Mechanics and Pyhsics of Solids.* vol. 54, n°11, pp. 2242-2280.

John W. Hutchinson, Z. X. 2003. Preliminary assesment of sandwich plates subject to blast loads. *International Journal of Mechanical Sciences* 45: 687–705.

Kolsky, H. 1949. An Investigation of the Mechanical Properties of Materials at Very High Rates of Strain. *Proc. Roy. Phys. Soc.* B 62 676-700.

Land Mine Survivors Network. http://www.landminesurvivors.org.

Micheal J. Mullin, B. J. O. T. 2004. Simulation of Energy Absorbing Materials in Blast Loaded Structures. *8th International LS-DYNA User Conference.*

Mukherjee, A. 1999. Layered sacrificial claddings under blast loading Part II-experimental studies. *International Journal of Impact Engineering*. Volume 24, Number 9, pp. 975-984(10).

Organization, R. A. T. 2004. Test Methodolgies for Personal Protective Equipment against Anti-Personal Mine Blast-Final report of the RHO Human Factors and Medicine Panel.

Stamatios A. Papadakis, M., PhD;1 Eleni C. Babourda, M. S. M. Thomas C. Mitsitskas, Costas Bachtis. 2006. Anti-personnel Landmine Injuries during Peace: Experience in a European Country.

Tasdemirci, A. 2007. High Strain Rate Reloading Compression Testing of a Closed-cell Aluminum Foam. *25. Impact/Crash and Other Dynamic Test Applications for Metallic Materials.*

Vaidya, R. S. a. U. K. 2004. Blast Impact on Aluminum Foam Composite Sandwich Panels. *8th International LS-DYNA User Conference*.

Veldman, R. l. 2004. Effects of Pre-Pressurization on Plastic Deformation of Blast-Loaded Square Aluminum Plates. *8th International LS-DYNA User Conference.*

Vinson, J. R. 2005. Sandwich Structures: Past, Present, and Future. Invited plenary speech at the *Seventh International Conference on Sandwich Structures, Sandwich Structures 7: Advancing with Sandwich Structures and Materials*, University of Aalborg, Denmark, pp. 3-12.